NASA CONTRACTOR REPORT

NASA CR-1406

MEASUREMENTS OF NEGATIVE ION PRODUCTION IN ATMOSPHERIC GASES

Prepared by
Dolores E. Ali, Consultant
Berkeley, Calif.
for Ames Research Center

NATIONAL AERONAUTICS AND SPACE ADMINISTRATION • WASHINGTON, D. C. • OCTOBER 1969

NASA CR-1406

MEASUREMENTS OF NEGATIVE ION PRODUCTION IN ATMOSPHERIC GASES

Prepared under Contract No. NAS 2-5209 by
Dolores E. Ali, Consultant
Berkeley, Calif.

for Ames Research Center

NATIONAL AERONAUTICS AND SPACE ADMINISTRATION

For sale by the Clearinghouse for Federal Scientific and Technical Information
Springfield, Virginia 22151 – CFSTI price $3.00

MEASUREMENTS OF NEGATIVE ION PRODUCTION IN ATMOSPHERIC GASES

by Dolores E. Ali

SUMMARY

Two electron capture by H^+ and He^+ in collisions with various gases has been investigated. The method used to measure effective cross sections for the charge changing reactions allows direct determination of the energy defects. Preliminary cross sections were obtained for two electron capture by H^+ at 0.28 keV and for H^+ and He^+ at 2 keV. In addition, negative ions formed by electron bombardment of gases in the ion source were mass analyzed; the results of this survey are summarized in the Appendix.

The charge exchange gases used in the cross section measurements were H_2, N_2, O_2, Kr, and Xe for H^+ at 2 keV; Kr, He, H_2, N_2, and O_2 for He^+ at 2 keV; and H_2, O_2, and Xe for H^+ at 0.28 keV. The corresponding cross sections range from 10^{-19} to 10^{-17} cm^2 for H^+ at 2 keV; 10^{-23} to 10^{-21} cm^2 for He^+ at 2 keV; and 10^{-21} to 10^{-19} cm^2 for H^+ at 0.28 keV. Finally, an attempt was made to observe two electron capture by N^+ at 2 keV; the results were inconclusive.

INTRODUCTION

Current interest in the production of negative ions derives from photometric studies of high temperature plasmas in shock tubes and in arcs. Analysis of the continuum radiation emitted by nitrogen plasmas, for example, has led to the suggestion of a stable N^- ion (ref. 1). However, most theoretical calculations by means of isoelectronic extrapolation indicate a negative binding energy for the ^3P ground state of the N^- ion (ref. 2). Although calculations do show a positive binding energy for the ^1D state of the N^- ion (ref. 3), a bound excited state may be insufficient to account for the anomalous radiation emitted by nitrogen plasmas.

In support of these spectroscopic studies, an experimental program was initiated at the Ames Research Center to investigate collision processes for negative ion production by using the 4 kV ion accelerator in the Physics Branch. It was decided to study in detail the process of two electron capture by singly charged positive ions for several reasons. First, two electron capture may be a more efficient process for the production of

negative ions than capture of free electrons by neutral atoms (ref. 4).

Second, direct observation of the N^- ion has been reported by Fogel', Kozlov, and Kalmykov (see ref. 4), who measured a cross section of approximately 10^{-22} cm^2 for the reaction N^+ to N^- in krypton at an N^+ beam energy of 34 keV. An independent observation of the N^- ion at a lower primary beam energy would serve to confirm its existence, and might provide information about the state of the negative ion.

Third, the process of two electron capture is ideally suited to the study of the shape of the function $\sigma(v)^*$ in the adiabatic region. The adiabatic region is defined by the condition $a|\epsilon|/hv \gg 1$, where a is the effective range of the interaction and ϵ is the change in internal energy of the particles (ref. 5). In the adiabatic region cross sections should increase with velocity according to the formula (ref. 6):

$$\sigma(v) \sim \exp\left[-\frac{k' a|\epsilon|}{hv}\right],$$

where k' is a constant. Deviations of $\sigma(v)$ from the adiabatic formula above have led to proposals that either the effective interaction range (a) is velocity-dependent or the relative velocity (v) is altered by the field of the interaction potential (ref. 7).

Of all the charge changing processes, ordinary charge exchange has the largest cross section. In general, it is two orders of magnitude larger than the cross section for two electron capture by singly charged positive ions. But, the state of excitation of the negative ion product of the two electron capture reaction is known and limited; thus, distortion of the $\sigma(v)$ curve is minimal. Since the adiabatic region is attained at low velocities, measurements of two electron capture cross sections at low impact energies are required.

Because the cross section for conversion of N^+ to N^- was expected to be small at low energies, preliminary measurements of the corresponding cross sections for H^+ and He^+ were made to establish calibration standards and experimental procedures. Since helium forms a long-lived negative ion only in an excited state (ref. 8), and atomic nitrogen may be similar in this respect, a study of the He^- ion was considered particularly useful. Results of the cross section measurements for H^+ and He^+ at impact energies of 0.28 keV and 2 keV are found in the main body of this report. The Appendix contains a brief summary of positive and negative ion formation by electron bombardment of atmospheric gases, nitric oxide, and carbon monoxide.

---

* $\sigma(v)$ is the effective cross section for an atomic collision process, and v is the relative velocity of the colliding particles.

There has been only one reported measurement of the two electron capture cross section for H^+ below 0.5 keV (ref. 9), and none for He^+ below 3 keV. The main experimental limitation has been detection of the small negative ion currents, a problem overcome in our experiments by applying multi-channel analyzer techniques.

APPARATUS AND EXPERIMENTAL METHOD

A schematic diagram of the apparatus used for the negative ion studies reported here is shown in figure 1. A detailed description of the ion accelerator may be found in reference 10.

Positive ions are formed by electron bombardment in a Carlston-Magnuson type ion source (ref. 11); the source is held at a positive potential with respect to ground (V_p), and the filament at a negative potential (V_e) with respect to the source chamber. The extracted ions pass through an electrostatic lens into a 90° magnetic analyzer, where they are separated by their charge to mass ratios. A second electrostatic lens then focuses the mass analyzed ion beam into the reaction chamber, C.

The reaction by which positive ions are converted into negative ions may be represented by the equation

$$X^+ + Y \rightarrow X^- + Y^{++} + |\epsilon| \ , \qquad (1)$$

where X^+ is the incident particle; Y, the target particle; and ϵ, the energy defect.

The mixed beam of unscattered particles emerging from the reaction chamber consists mainly of primary ions (X^+), neutral particles (X^o) formed by ordinary charge exchange, and negative ions (X^-) formed by two electron capture. The content of the beam may be expressed by the differential equations

$$\frac{dI^+}{dx} = -n(\sigma_{10} + \sigma_{1-1})\, I^+ + n\sigma_{01}\, I^o + n\sigma_{-11}\, I^- \ , \qquad (2a)$$

$$\frac{dI^o}{dx} = n\sigma_{10} I^+ - n(\sigma_{01} + \sigma_{0-1})\, I^o + n\sigma_{-10}\, I^- \ , \qquad (2b)$$

$$\frac{dI^-}{dx} = n\sigma_{1-1} I^+ + n\sigma_{0-1} I^o - n(\sigma_{-11} + \sigma_{-10})\, I^- \ , \qquad (2c)$$

where I^+, I^o, and I^- are respectively the positive, neutral, and negative currents in the beam; σ_{ij} is the effective cross section for the change of charge state from i to j; n is the number density of target gas particles; and x, the path length.

The solution of equation 2c when all quantities except I^+ are initially zero yields an expression for σ_{1-1} in terms of experimentally determined quantities. For thin targets the following formula is obtained:

$$I^- = I_o^+ n\sigma_{1-1} L , \qquad (3)$$

where I_o^+ is the initial value of I^+, and L is the effective path length of the reaction chamber.

At the exit to the reaction chamber is a parallel plate capacitor, D, that may be used to deflect charged particles from the beam. Following the deflector plates is a retarding chamber, R, originally intended for use in merging beams type experiments, but used here to retard the primary beam of positive ions when necessary. Beyond the chamber R is a triple stage electrostatic analyzer, A, set to pass negative ions of a specified energy, E_A, on to the single particle detector, EMT. (A collector, S, located near the entrance to the triple analyzer is used to measure positive ion currents.) The single particle detector at the exit to the triple analyzer is a 14-stage electron multiplier with copper-beryllium dynodes.

Figure 2 shows a block diagram of the electronics used in the detection system. Signal pulses from the electron multiplier pass through a pre-amplifier-discriminator-amplifier system; and the amplified pulses are counted by using a multi-channel analyzer, MCA, operated in the scaler mode.

In actual operation, the triple electrostatic analyzer is tuned to the primary energy; i.e., $E_A = E_p$. Therefore, the potential of the reaction chamber must be adjusted to a value that compensates for the energy lost by the incident particle during the reaction X^+ to X^-. If V_c represents the potential applied to the reaction chamber when the negative ion signal is observed, the conservation of energy and momentum equations may be used to derive an expression for $|\epsilon|$ (see eqn. 1) in terms of V_c. For forward scattering, the expression obtained is

$$\left[\frac{M}{m+M}\left(\frac{M}{m+M}E_i - |\epsilon|\right)\right]^{\frac{1}{2}} = \left[E_A - |qV_c|\right]^{\frac{1}{2}} - \frac{m}{m+M}E_i^{\frac{1}{2}} , \qquad (4)$$

where M and m are respectively the masses of the target and the incident particles; E_A is the energy for which the triple analyzer is set; E_i is the initial energy of the incident particles and it equals $E_p + |qV_c|$; and q is the electronic charge.

Automatic modulation of the parameter V_c is coupled with the multi-channel analyzer to improve the sensitivity of detection and to record the variation of signal with V_c (see fig. 2). The sawtooth output of an oscilloscope may be used to supply a sweep voltage of 140-volt range to the reaction chamber; this sweep must be synchronized to the channel advance sweep of the multi-channel analyzer.

CROSS SECTION MEASUREMENTS FOR H^+ AT 0.28 keV

Experimental Procedure

Approximately 10 mμA of H^+ reaches the collector, S, near the entrance to the triple analyzer when the source pressure is 5×10^{-4} torr of H_2 and the electron bombardment energy is 90 eV. Once the current to S has been measured, positive potentials are applied to the plates of the triple analyzer; and these plate voltages are adjusted to optimize the current reaching the first dynode of the electron multiplier, D1. The transmission of the analyzer, or the ratio of I^+_{D1} to I^+_o, is measured during the "tuning" procedure. Then the plate voltages are switched to opposite polarity to set the triple analyzer for 0.28 keV negative ions.

After the triple analyzer has been tuned, gas is admitted to the reaction chamber until the H^+ current to S is reduced to half its initial value. Then the H^- signal counts are accumulated for a fixed number of sweeps of the voltage V_c. The counting procedure is repeated twice, once with the ion beam deflected and once with the gas off, in order to subtract from the signal any background noise from the neutrals and positive ions in the beam. To minimize background noise from the positive ions, the retarding chamber, R, is held at a positive potential above ground (+300 V) during the counting procedure.

Method of Data Analysis

The two electron capture cross section , σ_{1-1}, is calculated by using the equation 3 and the following formulas:

$$I^- = \frac{q\,C^-}{\xi T}\,, \tag{5a}$$

$$n = 3.28 \times 10^{16}\, p\,, \qquad (5b)$$

where q is the electronic charge in coulombs; C^-, the number of negative ion counts per second measured at the peak of the signal distribution curve; ξ, the efficiency of the detector; τ, the transmission of the triple analyzer; and p, the pressure in torr inside the reaction chamber. In equation 3, L is the length of the reaction chamber in cm (= 13.5 cm), and σ_{1-1} is the cross section in cm^2. All currents are in amperes.

The primary current, I_o^+. -- The current is measured at the entrance to the triple analyzer, rather than at the entrance to the reaction chamber, in order to account for current and signal losses from defocusing of the beam between these two points. Since a positive potential is applied to chamber R (see fig. 1) during the counting procedure, the opposite polarity is applied when I_o^+ is measured in order to account for any focusing effect V_R has on the signal. The collector, S, is held at $+22\frac{1}{2}$ V to suppress secondary electron emission when the current is measured. Also, the reaction chamber (C) is grounded and there are no background gases admitted. Residual pressures in the accelerator are less than 10^{-7} torr.

Negative Ion Counts, C^-. -- Since the range of energies accepted by the triple analyzer is considerably wider than the energy dispersion of the beam, the signal counts are taken from the peak of the distribution curve rather than from the area under the curve. Typical distribution curves are shown in figure 3. A retarding potential analysis of the 0.28-keV primary beam indicates a full width at half maximum of 2 eV.

Pressure, p. -- The pressure is monitored by a Bayard-Alpert ionization gauge located near the reaction chamber. A McLeod gauge must be used to determine absolute pressure. But, since this pressure calibration would have disrupted operation of the ion accelerator, it was deferred to a more convenient time. Instead, we have used in the present analysis pressure calibration data taken by Savage and Witteborn in the course of their N_2^{++} experiment (see ref. 12), which was done on the same apparatus. Ionization gauge pressures (p_i) for all gases have been calibrated against their result for N_2 at $p_i = 2.00 \times 10^{-5}$ torr, where the corresponding McLeod gauge reading is $p = 1.30 \times 10^{-3}$ torr at $T = 22.4^{\circ}C$. This determines experimentally the impedance (β) of the reaction chamber; viz., $\beta = 65$. Absolute pressures (p) then are calculated by multiplying relative pressures (p_i) by two factors: β, the impedance or differential pumping factor; and γ, an adjustment to the ionization gauge reading for the sensitivity of the gauge to the particular gas used. The "gauging" factors for a gauge reading of 1.00 are listed below:

TABLE I. - GAUGING FACTORS

Gas	γ	Gas	γ
N_2	1.00	O_2	1.20
Air	1.00	He	4.80
Ar	0.66	Kr	0.52
H_2	2.40	Xe	0.37

These factors lie within 10 percent of those given by Dushman (ref. 13) for a standard gauge, with the exception of γ for argon.

Since the cross section measurements reported here were made at only one pressure, an investigation of the pressure dependence of the observed signals must be made to confirm that the negative ions result from single collisions.

Transmission, τ. -- The transmission of the triple analyzer is the ratio of I^+_{D1} to I_o^+, where I^+_{D1} is the current to the first dynode of the electron multiplier. A potential of -250 V on the screen dynode (D-0) in front of D1 is sufficient to suppress secondary electron emission during the current measurement. Approximately twenty percent of the beam is transmitted through the triple analyzer.

Efficiency, ξ. -- When negative ions are detected, the screen dynode is connected through a potential divider circuit to the anode of the electron multiplier; the applied potentials are +250 V to D-0 and +3500 V to the anode. To detect positive ions, D-0 is disconnected from the divider circuit; and the following potentials are applied: -250 V to D-0, -450 V to D1, and +2600 V to the anode. In both cases, the potential drop across the electron multiplier is +3050 V; and the ions impact D1 at 730 eV.

The efficiency of the detector was measured for the positive ion, and the assumption was made that the corresponding negative ion would be detected with the same efficiency.

The measurement of ξ would have been a straightforward comparison of I^+_{D1} with the corresponding counts per second had a more sensitive ammeter been available at the time. Instead, it was necessary to obtain curves of I^+_{D1} versus a retarding voltage, and then to relate these to similar curves for the counts per second. The best estimate of ξ from these measurements is $\xi = 0.065 \pm 0.020$ when the potential drop across the multiplier is

+3050 V. Extrapolation of the retarding potential curves is responsible for the large uncertainty in ξ.

Results and Discussion

Measurements were made for the reaction H^+ to H^- in hydrogen, oxygen, and xenon at an H^+ beam energy of 0.28 keV. The cross sections are listed below, along with the estimated standard deviations:

TABLE II. - TWO ELECTRON CAPTURE CROSS SECTIONS FOR H^+ AT 0.28 keV

Target gas	σ_{1-1}, cm^2
H_2	$(4.7 \pm 1.7) \times 10^{-21}$
O_2	$(2.4 \pm 0.8) \times 10^{-20}$
Xe	$(1.3 \pm 0.5) \times 10^{-19}$

Errors in σ_{1-1} arise from uncertainties in the parameters of equations 3 and 5. The values of these uncertainties were estimated to be: $\Delta L/L = 0.05$, $\Delta\tau/\tau = 0.10$, $\Delta I^-/I^- = 0.05$, $\Delta\xi/\xi = 0.30$, $\Delta p/p = 0.10$,* and $\Delta I_o^+/I_o^+ = 0.10$.

If the transmission is measured just prior to the counting procedure, σ_{1-1} may be calculated from the following equation.

$$I^- = \xi I_{D1}^+ n\sigma_{1-1} L , \qquad (6)$$

obtained by substitution of I_{D1}^+/I_o^+ for τ. This procedure was used to measure the cross section for H^+ in xenon; the uncertainty in I_{D1}^+ was approximately 0.05.

The cross section listed above for H^+ in hydrogen is approximately a factor of two smaller than that obtained by Kozlov and Bondar at 0.15 keV (ref. 9). Their results for H^+ in H_2 from 0.15 to 5 keV are graphed in

* The uncertainty in p quoted here does not include errors in the gauging factor (γ) and the impedance (β).

figure 4; the original paper should be consulted for exact values. Since our experimental method does not allow for large angle scattering, this discrepancy is understandable. Apparently Kozlov and Bondar measured the total cross section by means of a modified mass spectrometric method similar to that described in reference 14.

The experimental method described in this report allows simultaneous determination of σ_{1-1} for forward scattering and ϵ, the energy defect of the charge changing reaction. If ϵ is known, the process by which the primary particle captures two electrons may be specified. This is particularly interesting in the case of molecular particles, for which the reaction may proceed either by double ionization of the target molecule or by a dissociative ionization process; i.e., either by the reaction $X^+ + Y_2 \rightarrow X^- + Y_2^{++} + |\epsilon|$ or by the reaction $X^+ + Y_2 \rightarrow X^- + Y^+ + Y^+ + |\epsilon'|$. As examples, we calculate ϵ for H^+ in H_2 and O_2 by comparison with ϵ for H^+ in Xe.

Differentiation of equation 4 gives:

$$\left[1 + \left(\frac{M}{m+M}\right)^2\right] \Delta V_c = - \left(\frac{M}{m+M}\right)^2 \Delta E_p \ , \qquad (7)$$

for small m/m+M. From the peak positions of the signal curves for H^+ in xenon at E_p = 240 eV and E_p = 280 eV when E_A = 280 eV (see fig. 5), we calculate approximately 0.8 V per channel. If $|\epsilon(Xe)|$* for H^+ in xenon is equal to 19 eV, then we calculate $|\epsilon(H_2)|$ = 28 eV and $|\epsilon(O_2)|$ = 26 eV (for H^+ in H_2 and O_2) by using equation 4 and the peak positions shown in figure 3. These values may be compared to the internal energy defects for the reactions $H^+ + H_2 \rightarrow H^- + H^+ + H^+$ [$\epsilon(H_2)$] and $H^+ + O_2 \rightarrow H^- + O_2^{++}$ [$\epsilon(O_2)$]; $|\epsilon(H_2)| = |E_H^I + S_H - E_{diss} - 2E_H^I - E_{pot}|$ = 35 eV if the potential energy of the two protons (E_{pot}) is 18 eV (ref. 15), and $|\epsilon(O_2)| = |E_H^I + S_H - E_{O_2}^{II}|$ = 22 eV if the threshold energy for O_2^{++}($E_{O_2}^{II}$) is 36 eV (ref. 16).

The energy defect $\epsilon(H_2)$ that we calculate from equation 4 seems to indicate a smaller value for the quantity E_{pot}. However, uncertainty in the measurement of V_c may be responsible for the discrepancy between the energy defects calculated from equation 4 and those estimated from the threshold

---

* The internal energy defect is equal to $|E_H^I + S_H - E_{Xe}^{II}|$ where E_H^I is the threshold for H^+; S_H is the electron affinity of H^-(= 0.75 eV); and E_{Xe}^{II} is the threshold for Xe^{++}.

potentials and S_H(and E_{pot} where applicable). Since the results quoted here are preliminary, it is expected that more accurate values for the energy defects will be obtained when these experiments are repeated.

CROSS SECTION MEASUREMENTS FOR H^+ AND He^+ AT 2 keV

Experimental Procedure

The experimental procedure at 2 keV is similar to that previously described for H^+ at 0.28 keV. Typical currents were 250 mμA of He^+ and 50 μμA of H^+. Source pressures were on the order of 10^{-4} torr; and the electron bombardment energies were 187 eV and 137 eV for He^+ and H^+ respectively.

Because the triple electrostatic analyzer was designed mainly for use with low energy ion beams, there were frequent voltage breakdowns when the high potentials needed for discrimination of a 2 keV beam were applied to the analyzer plates. The resulting loss of resolution and fluctuations in the transmission are primarily responsible for the large uncertainties in the data that follow. Also, shifting of the signal peak position made it impossible to determine a unique V_c for each reaction.

Background noise from the positive ions was low enough that the retarding chamber in front of the triple analyzer was not used; it was kept at ground potential.

The sweep voltage applied to the reaction chamber ranged from -70 to +70 V. It was observed that the positive voltages defocused the primary beam (see fig. 6). Although the effect on the negative ion signal is not certain, positive voltages (V_c) appear to have had an opposite, or focusing, effect on the negative ions. However, the transmission of the triple analyzer did not vary greatly with V_c (see fig. 6).

Method of Data Analysis

Again, the two electron capture cross sections for H^+ and He^+ at 2 keV were calculated from the relationship $q\,C^- = 3.28 \times 10^{16} \xi\tau\, I_o^+\, p\, L$, obtained by combining equations 3 and 5.

Efficiency, ξ. -- The efficiency of the detector was estimated to be 0.09 and 0.30 when the applied voltages were respectively +3000 V and +3500 V to the anode and -100 V to D-O.

Pressure, p. -- Pressures in the reaction chamber were calculated by multiplying the relative pressures, p_i, by $\gamma\beta$. Table I lists the values

used for γ. The impedance, β, has a value of 65 except for N_2 at $p_i = 2.8 \times 10^{-5}$ torr, $\beta = 66$; for H_2 at $p_i = 3.2 \times 10^{-5}$ torr, $\beta = 68$; for H_2 at $p_i = 3.9 \times 10^{-5}$ torr, $\beta = 71$; and for Xe at $p_i = 2.0 \times 10^{-5}$, $\beta = 56$.

Results and Discussion

For the reaction H^+ to H^- in hydrogen, the cross section is 5×10^{-19} cm^2 with a standard deviation of 3×10^{-19} cm^2. The quoted error reflects uncertainties in I^-, I_o^+, p, ξ, L, and τ; it does not include errors in β and γ nor those due to defocusing effects. Approximate values for the uncertainties in the parameters above are: $\Delta I^-/I^- \sim 0.45$, $\Delta I_o^+/I_o^+ \sim 0.05$, $\Delta p/p \sim 0.10$, $\Delta\xi/\xi \sim 0.30$, $\Delta L/L \sim 0.05$, and $\Delta\tau/\tau \sim 0.25$. The H^- counts varied by about a factor of two under the same experimental conditions; and the value listed above for $\Delta I^-/I^-$ reflects this variation although the cause is undetermined. The relative cross sections for H^+ in N_2, O_2, Kr and Xe are tabulated below:

TABLE III. - RELATIVE TWO ELECTRON CAPTURE CROSS SECTIONS FOR H^+ AT 2 keV

Target gas	σ_r, 5×10^{-19} cm^2
Xe	24
Kr	10
O_2	3
N_2	0.9

Comparison with the results obtained by Kozlov and Bondar (ref. 9) for H^+ in H_2, by Fogel (ref. 7) for H^+ in Xe, and by Kozlov et al. (ref. 17) for H^+ in Kr indicates that our measurements may be too large by about a factor of two (see fig. 4).

The cross section for two electron capture by He^+ in helium is 8×10^{-23} cm^2. A standard deviation of 4×10^{-23} cm^2 is calculated by using the uncertainties in I_o^+, p, ξ, L, and τ listed above and $\Delta I^-/I^- \sim 0.15$. Relative cross sections for He^+ in H_2, N_2, O_2, and Kr are listed below:

TABLE IV. - RELATIVE TWO ELECTRON CAPTURE CROSS SECTIONS FOR He^+ AT 2 keV

Target gas	σ_r, 8×10^{-23} cm^2
O_2	25
N_2	10
H_2	1.6
Kr	0.3

There are no other measurements of σ_{1-1} for He^+ at 2 keV with which to compare our results. Windham et al. (ref. 18) measured a cross section of $\sim 10^{-20}$ cm^2 for He^+ in hydrogen at an He^+ beam energy of 17.5 keV; the results of Dukel'skii et al. (ref. 19) for He^+ in helium and krypton are graphed in figure 7.

A cursory investigation of the variation of cross section with electron accelerating potential was made for He^+ in He. As shown below, the cross section increases by about 25 percent when V_e is increased from 37 V to 187 V:

V_e, volts	σ_{1-1}, 10^{-23} cm^2
37	6.4
87	6.6
137	6.9
187	8.0

Typical negative ion signal curves are shown in figures 8 and 9. The structure visible in these curves may be due to instrumental effects, but further investigation is necessary before a satisfactory explanation can be given.

CROSS SECTION MEASUREMENTS FOR "N^+" AT 2 keV

After the capability of the technique for producing the metastable He^- ion had been demonstrated, the next step was to attempt production of N^-.

A beam of N^+ (~ 5 mμA) was obtained from N_2 at a source pressure of approximately 10^{-4} torr and at an electron bombardment energy of 187 eV. The 2-keV N^+ beam was sent through three different charge exchange gases, and in each case negative ions were observed. The relative signals obtained ($I^-/I_o{}^+p$) and the charge exchange gases used are listed below:

Gas	Signal, 10^{-4} per torr
Kr	3.6
O_2	0.7
N_2	0.5

These signals correspond to two electron capture cross sections of 8×10^{-22} cm^2 to 1×10^{-22} cm^2. However, to assure that the observed signal resulted from N^+ and not from impurities in the beam, the analyzer field was varied while source and focusing conditions were kept constant. As the field was adjusted toward higher q/m - values, and as the N^+ current accordingly decreased, the signal was observed to increase. Figure 10 shows the curves for N^+ current and for the I^- signal versus B; B is the magnetic field in gauss measured external to the analyzer magnet chamber, and thus it is only proportional to the actual bending field. Therefore, it was concluded that the negative ion signal probably resulted from O^+, OH^+, and F^+ contaminants in the N^+ beam. Since only high purity (99.95 percent) or research grade (99.999 percent) gases were used, the impurities are due mainly to gases evolved from the filament or the walls of the source chamber. Although a positive ion spectrum of the primary beam showed that it contained less than 6 percent O^+ and 3 percent F^+ (see the Appendix and fig. 12), the two electron capture cross sections for O^+ and F^+ are large enough to account for the observed negative ion signal.*

* Fogel (see ref. 7) gives $\sigma_{1-1} = 8.8 \times 10^{-17}$ cm^2 for F^+ in Kr at about 6 keV and $\sigma_{1-1} = 4.4 \times 10^{-17}$ cm^2 for O^+ in Kr at about 11.5 keV.

APPENDIX

SURVEY OF IONS EMITTED FROM THE SOURCE

A more direct method for the study of negative ion production may be mass analysis of ions emitted from the source. Although in the past the mass spectrometric method has not yielded information about the N^- ion, the increased sensitivity of our detection system required that it be tried. A number of reactions are responsible for negative ion production in the source, including dissociative ionization, charge exchange, and single electron capture of slow secondary electrons.

Mass analysis was achieved by using the analyzer magnetic field as the sweep parameter coupled with the multi-channel analyzer.* Since there were no charge exchange gases used, residual pressures in the accelerator were about 10^{-8} torr. Chambers C and R in figure 1 were grounded; and the triple electrostatic analyzer was tuned to the primary energy, 280 eV.

Mainly to establish a mass scale, but also to determine the impurity content of the primary beam, positive ion spectra were obtained for O_2, N_2, and Ar; sources pressures were about 10^{-4} torr, and the electron bombardment energy was 90 eV. These spectra are shown in figures 11 through 13. The concave shape of the peaks identified as O_2^+, N^+, N_2^+, Ar^+, and Ar^{++} resulted from saturation of the detector.

Then, negative ion spectra were obtained by reversing the polarity of the potentials on the source chamber and focusing electrodes, and by reversing the direction of the magnetic field. Figures 14 through 19 show the spectra obtained for He, Air, N_2 (research grade), NO, CO, and O_2. There are several points of interest in the helium and nitrogen spectra: the mass 16 to 19 impurities in both; the absence of He^- from the helium spectrum (fig. 14); and the relatively large peak at mass 26 in the nitrogen spectrum (fig. 16).

It is possible that the impurities in nitrogen (O^-, OH^-, F^-) mask an N^- signal. But, because He^- was not observed, it is doubtful that N^- would be observed even with better mass resolution.

---

* Refer to the discussion under "Apparatus and Experimental Method" in the main body of this report for details of the detection system.

The mass 26 peak in the nitrogen spectrum has been identified tentatively as CN^-; the signal intensity varied in proportion to the nitrogen pressure in the source. Utterback (ref. 20) found that from 12 to 60 eV N_2 reacts with CO to form predominantly NO^+ and CN^-; and a similar reaction may account for the mass 26 peak in the nitrogen spectrum (fig. 16).

SYMBOLS

Δ	a difference operator; e.g., $\Delta X = X_1 - X_2$
ϵ	change in internal energy of a system resulting from collisions
k'	a constant
h	Planck's constant
v	relative velocity
$\sigma(v)$	cross section as a function of v
a	effective interaction range
V_p	source chamber voltage with respect to ground
V_e	filament bias voltage with respect to the source chamber
$\frac{d}{dx}$	the differential operator
x	effective path length of ions in the charge exchange gas
I^o	neutral current
I^+	positive ion current
I^-	negative ion current
n	number of molecules per unit volume in the reaction chamber
σ_{ij}	cross section for the change of charge from qi to qj where i = 1, 0, -1 and j = 1, 0, -1
q	electronic charge
I_o^+	the initial positive ion current measured at the entrance to the triple electrostatic analyzer
L	effective length of the reaction chamber
M	mass of the target molecule
m	mass of the projectile molecule

E_i	initial energy of the projectile ion in the reaction chamber
E_p	energy of the projectile before entering the reaction chamber
V_c	reaction chamber voltage
E_A	energy for which the triple electrostatic analyzer is tuned
C^-	number of negative ion counts per second
ξ	efficiency of the electron multiplier detector
τ	transmission of the triple electrostatic analyzer
I^+_{D1}	initial positive ion current measured at the entrance to the electron multiplier detector
p	absolute pressure of the charge exchange gas in the reaction chamber
p_i	relative pressure measured by using an ionization gauge
γ	gauging factor determined by the sensitivity of the ionization gauge to various gases
β	impedance of the reaction chamber
E_X^I, E_X^{II}	threshold energies for the singly and doubly charged positive ion of the molecule X
S_X	electron affinity of the neutral molecule X
E_{pot}	potential energy of two protons
σ_r	relative cross section

REFERENCES

1. Thomas, G. M.; and Menard, W. A.: Measurements of the Continuum and Atomic Line Radiation from High Temperature Air. AAIA J., vol. 5, Dec. 1967, pp. 2214-2223.

   Norman, G. E.: The Role of the Negative Ion N^- in the Production of the Continuous Spectrum of Nitrogen and Air Plasmas. translation: Opt. Spectry., vol. 17, No. 2, Aug. 1964, pp. 94-96.

   Allen, R. A.; and Textoris, A.: Evidence for the Existence of N^- from the Continuum Radiation from Shock Waves. J. Chem. Phys., vol. 40, no. 11, June 1964, pp. 3445-3446.

   Boldt, G.: Recombination and "Minus" - Continuum of Nitrogen Atoms. Z. Physik, vol. 154, 1959, pp. 330-338.

2. Edlen, B.: Isoelectronic Extrapolation of Electron Affinities. J. Chem. Phys., vol. 33, no. 1, June 1960, pp. 98-100.

   Johnson, H. R.; and Rohrlich, F.: Negative Atomic Ions. J. Chem. Phys., vol. 30, no. 6, June 1959, pp. 1608-1613.

3. Schaefer, Henry F., III; and Harris, Frank E.: Metastability of the ^1D state of the Nitrogen Negative Ion. Phys. Rev. Letters, vol. 21, no. 23, Dec. 1968, pp. 1561-1562.

   Bates, D. R.: and Moiseiwitsch, B. L.: Energies of Normal and Excited Negative Ions. Proc. Phys. Soc. London, series A, vol. 68, June 1955, pp. 540-542.

4. Fogel', Ya. M.; Kozlov, V. F.; and Kalmykov, A. A.: On the Existence of the Negative Nitrogen Ion. Zh. Eksperim. i. Teor., vol. 36, May 1959, pp. 1354-1356 (translation: Soviet Phys. - JETP, vol. 36(9), no. 5, Nov. 1959, pp. 963-964).

5. Massey, H. S. W.: Collisions Between Atoms and Molecules at Ordinary Temperatures. Rept. Progr. Phys., vol. 12, 1948, pp. 248-269.

6. Hasted, J. B.: Inelastic Ion-Atom Collisions. J. Appl. Phys., vol. 30, no. 1, Jan. 1959, pp. 25-27.

7. Fogel', Y. M.: The Production of Negative Ions in Atomic Collisions. Usp. Fiz. Nauk., vol. 71, June 1960, pp. 243-287 (translation: Soviet Phys. Uspekhi, vol. 3, No. 3, Nov. - Dec. 1960, pp. 390-416).

8. Holøien, E.; and Midtdal, J.: On a Metastable Energy State of the Negative Helium Ion. Proc. Phys. Soc. London, series A, vol. 68, 1955, pp. 815-823.

9. Kozlov, V. F.; and Bondar', S. A.: Double Charge Exchange Between Singly-Charged Positive Ions at Low Energies. Zh. Eksperim. i. Teor. Fiz., vol. 50, Feb. 1966, pp. 297-306 (translation: Soviet Phys. - JETP, vol. 23, no. 2, Aug. 1966, pp. 195-202).

10. Nichols, Billy J.: and Witteborn, Fred C.: Measurements of Resonant Charge Exchange Cross Sections in Nitrogen and Argon Between 0.5 and 17 eV. NASA TN D-3265, Feb. 1966.

11. Carlston, C. E.: and Magnuson, G. D.: High Efficiency Low Pressure Ion Source. Rev. Sci. Inst., vol. 33, no. 9, Sept. 1962, pp. 905-911.

12. Savage, H. F.: and Witteborn, F. C.: Charge-Exchange Cross Sections of N_2^{2+} in N_2, CO_2, and Ar and Contamination of N^+ Beams by N_2^{2+}. J. Chem. Phys., vol. 48, no. 4, Feb. 1968, pp. 1872-1873.

13. Dushman, Saul: Scientific Foundations of Vacuum Technique. Second ed., John Wiley and Sons, Inc., 1965, pp. 323-324.

14. Kozlov, V. F.: and Bondar', S. A.: Method for the Measurement of Double Charge-Exchange Cross Sections of Low-Energy Positive Ions. Zh. Tekh. Fiz., vol. 37, no. 3, March 1967, pp. 542-549 (translation: Soviet Phys. - Tech. Phys., vol. 12, no. 3, Sept. 1967, pp. 388-393).

15. Fogel', Ia. M.; and Krupnik, L. I.: The Formation of Negative Oxygen Ions in the Collisions of Positive Oxygen Ions with Gas Molecules. Zh. Eksperim. i. Teor. Fiz., vol. 29, August 1955, pp. 209-220 (translation: Soviet Phys. - JETP, vol. 2, no. 2, March 1956, pp. 252-261).

16. Dorman, F. H.; and Morrison, J. D.: Ionization Potential of Doubly-Charged Oxygen and Nitrogen. J. Chem. Phys., vol. 39, no. 7, Oct. 1963, pp. 1906-1907.

17. Kozlov, V. F.; Fogel', Ya. M.; and Stratienko, V. A.: Two-Electron Charge Exchange of Low-Energy Protons. Zh. Eksperim. i. Teor. Fiz., vol. 44, June 1963, pp. 1823-1825 (translation: Soviet Phys. - JETP, vol. 17, no. 6, Dec. 1963, pp. 1226-1227).

18. Windham, P. M.: Joseph, P. J.; and Weinman, J. A.: Negative Helium Ions. Phys. Rev., vol. 109, no. 4, Feb. 1958, pp. 1193-1195.

19. Dukel'skii, V. M.: Afrosimov, V. V.: and Fedorenko, N. V.: Zh. Eksperim. i. Teor. Fiz., vol. 30, April 1956, pp. 792-793 (translation: Soviet Phys. - JETP, vol. 3, 1956, pp. 764-766).

20. Utterback, Nyle G.: Cross Section for Atom Exchange with Charge Transfer in a Molecular Collision. J. Chem. Phys., vol. 44, no. 6, March 1966, pp. 2540-2541.

LIST OF FIGURES

Figure 14. - Typical mass spectrum of negative ions with helium in the ion source. Some main components are identified on the graph.

Figure 15. - Negative ion spectrum with air in the source.

Figure 16. - Negative ion spectrum with research grade nitrogen in the source.

Figure 17. - Negative ion spectrum with nitric oxide in the source.

Figure 18. - Negative ion spectrum with carbon monoxide in the source.

Figure 19. - Negative ion spectrum with oxygen in the source.

SCHEMATIC DIAGRAM ION ACCELERATOR AND END STATION

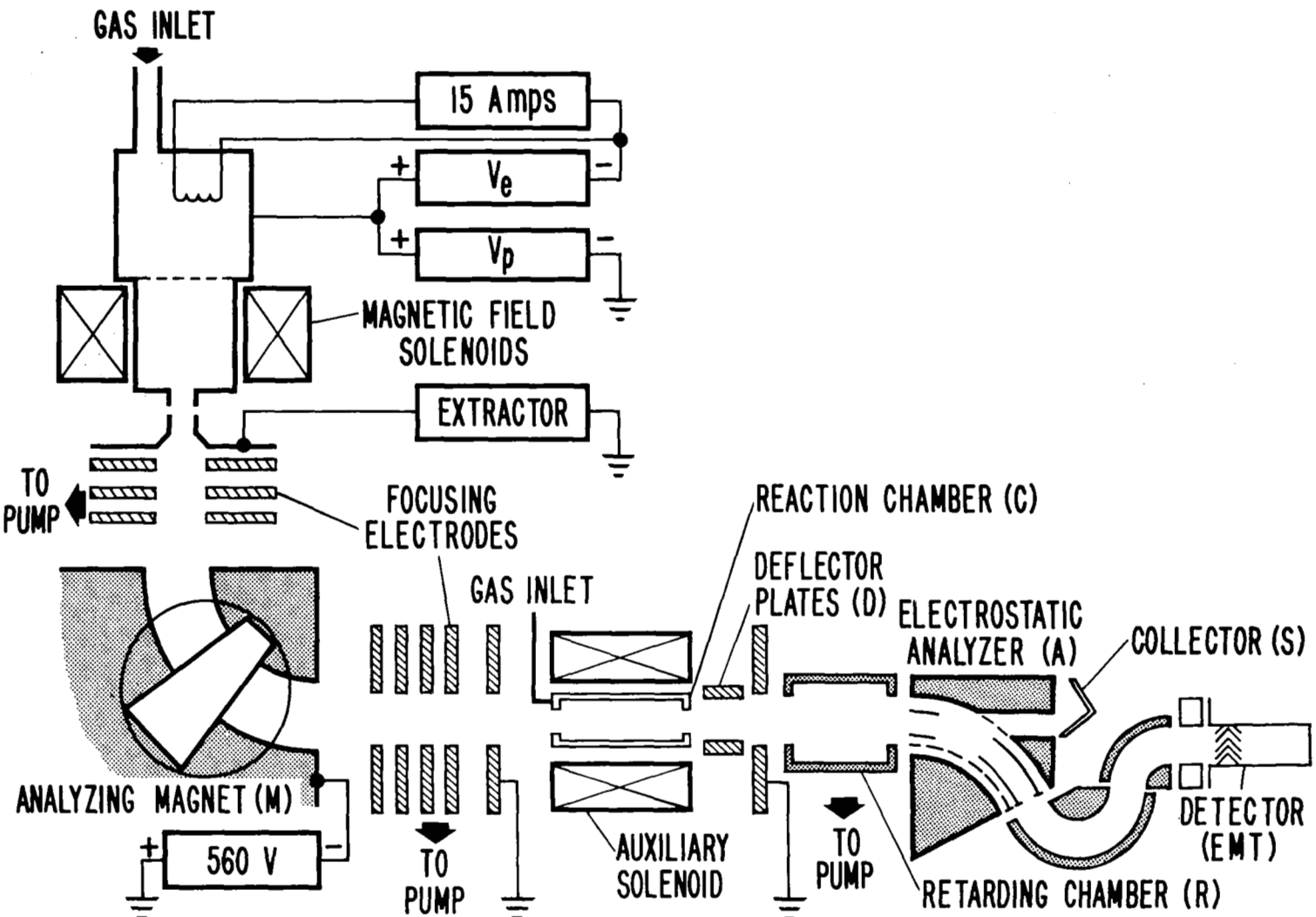

Figure 1

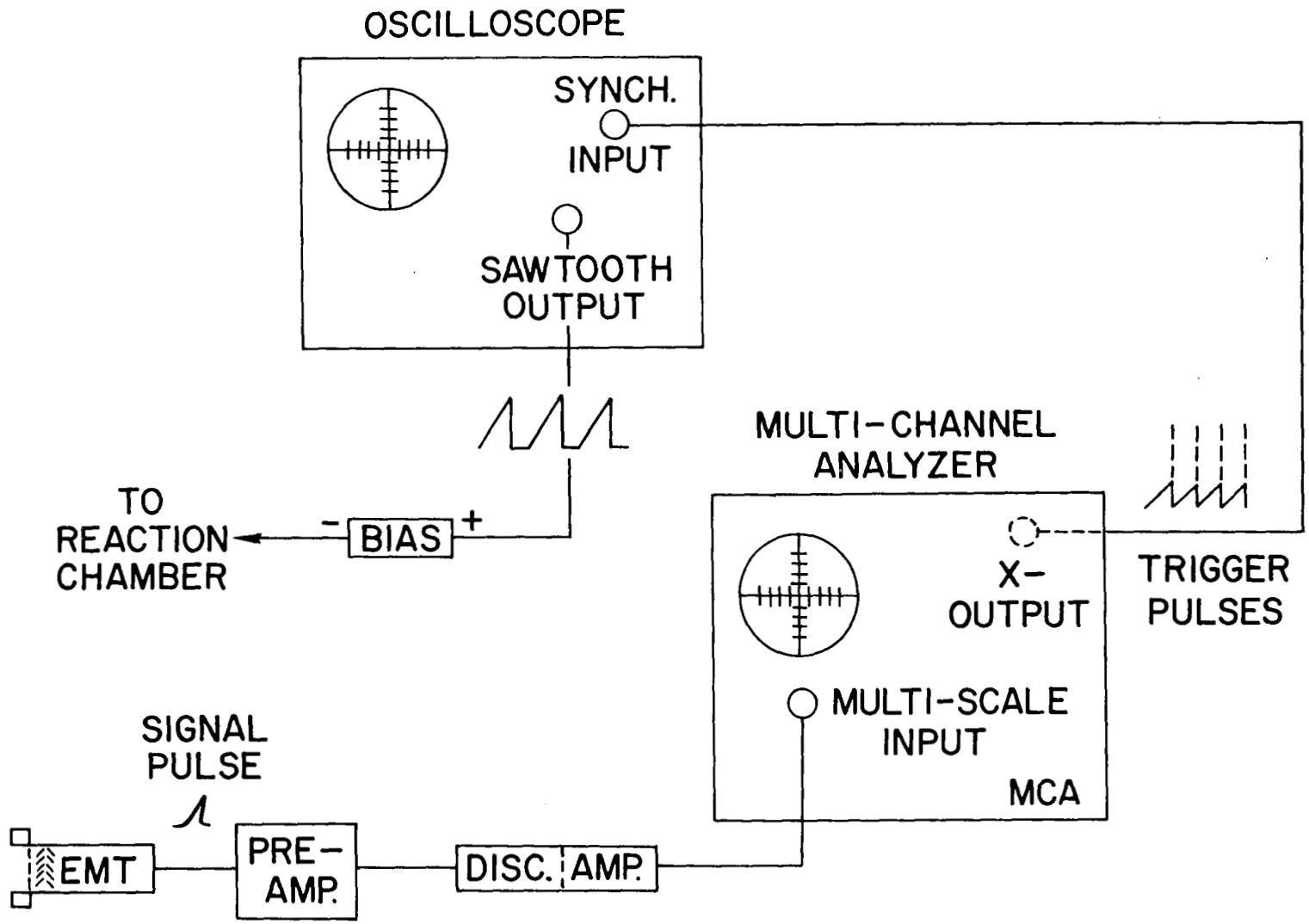
OSCILLOSCOPE
SYNCH.
INPUT
SAWTOOTH
OUTPUT
MULTI-CHANNEL
ANALYZER
TO
REACTION
CHAMBER
-
BIAS
+
X-
OUTPUT
TRIGGER
PULSES
MULTI-SCALE
INPUT
MCA
SIGNAL
PULSE
EMT
PRE-
AMP.
DISC.
AMP.

Figure 2

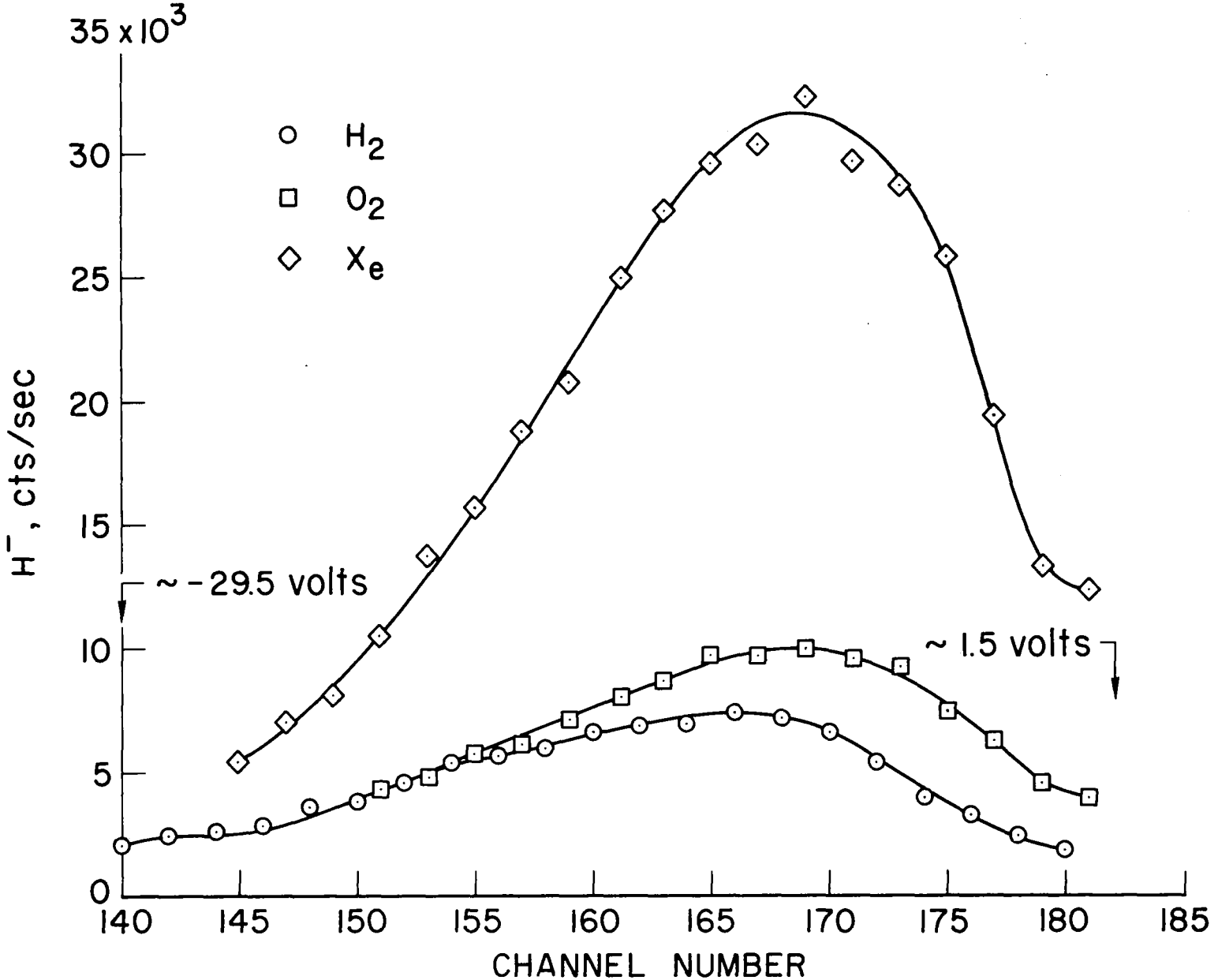
35 x 10^3
30
25
20
15
10
5
0
H⁻, cts/sec
H2
O2
Xe
~ -29.5 volts
~ 1.5 volts
140
145
150
155
160
165
170
175
180
185
CHANNEL NUMBER

Figure 3

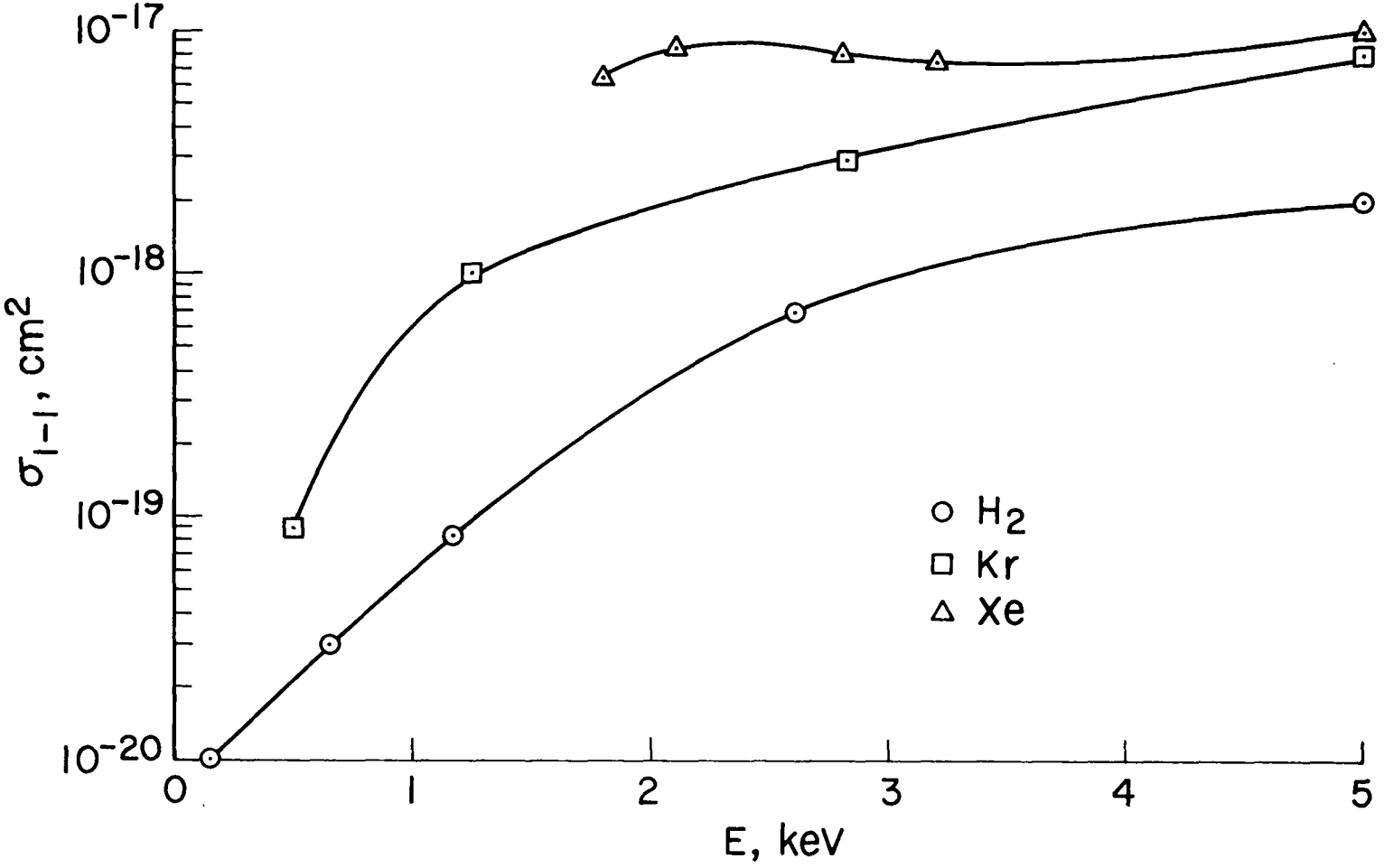

Figure 4

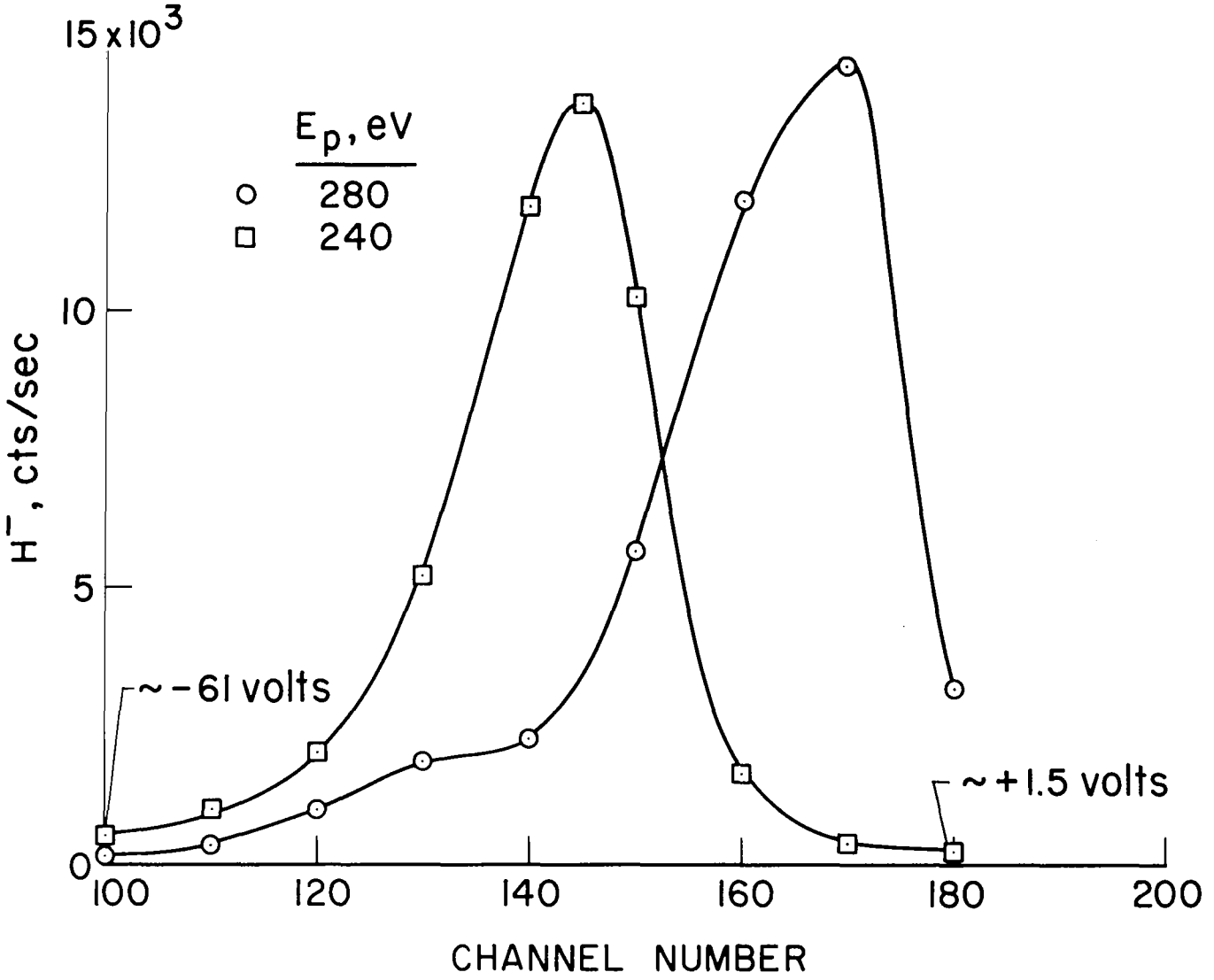
15 x 10^3
10
5
0
H⁻, cts/sec
Ep, eV
280
240
~ -61 volts
~ +1.5 volts
100
120
140
160
180
200
CHANNEL NUMBER

Figure 5

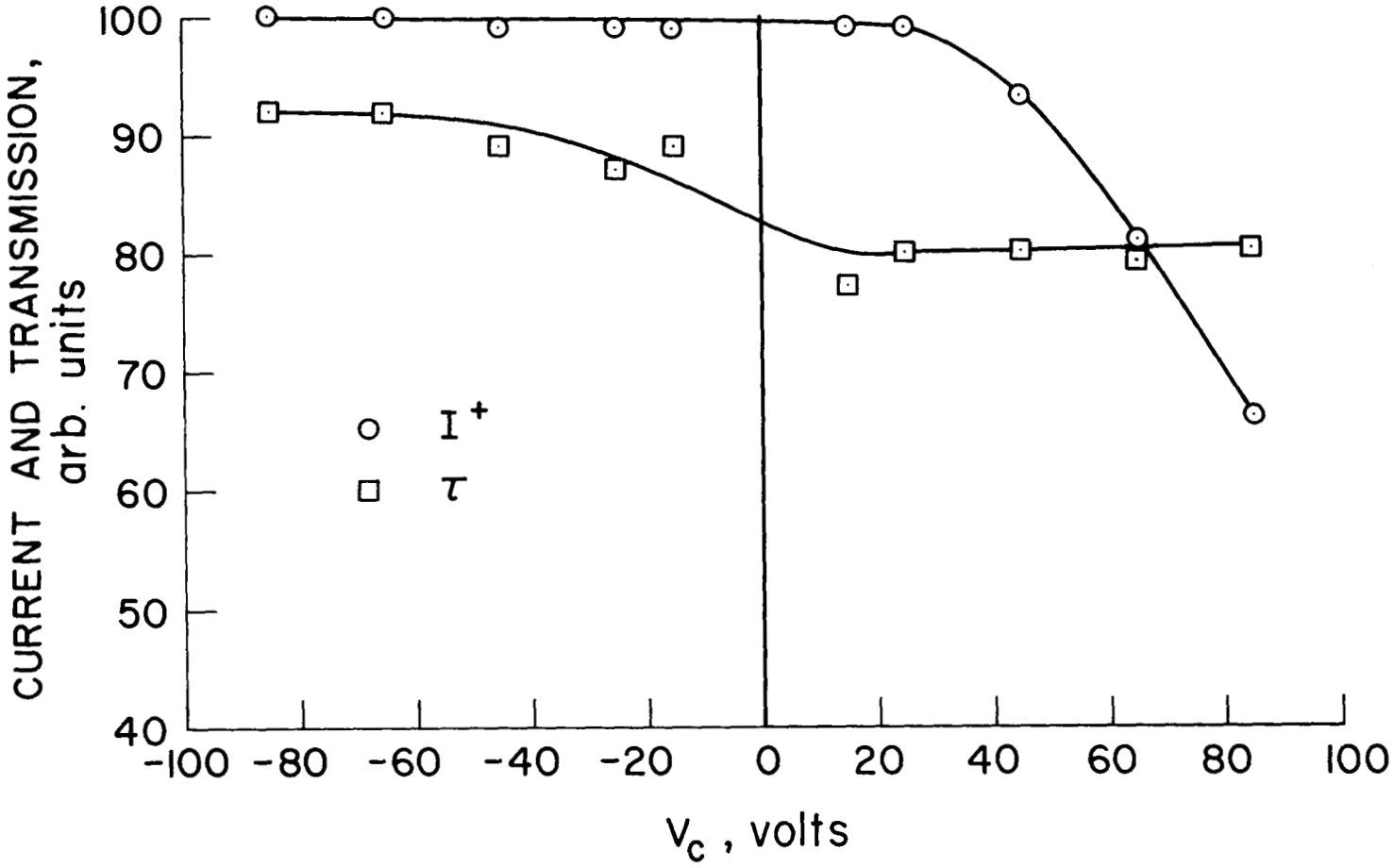
CURRENT AND TRANSMISSION, arb. units
100
90
80
70
60
50
40
-100
-80
-60
-40
-20
0
20
40
60
80
100
I^+
τ
V_c , volts

Figure 6

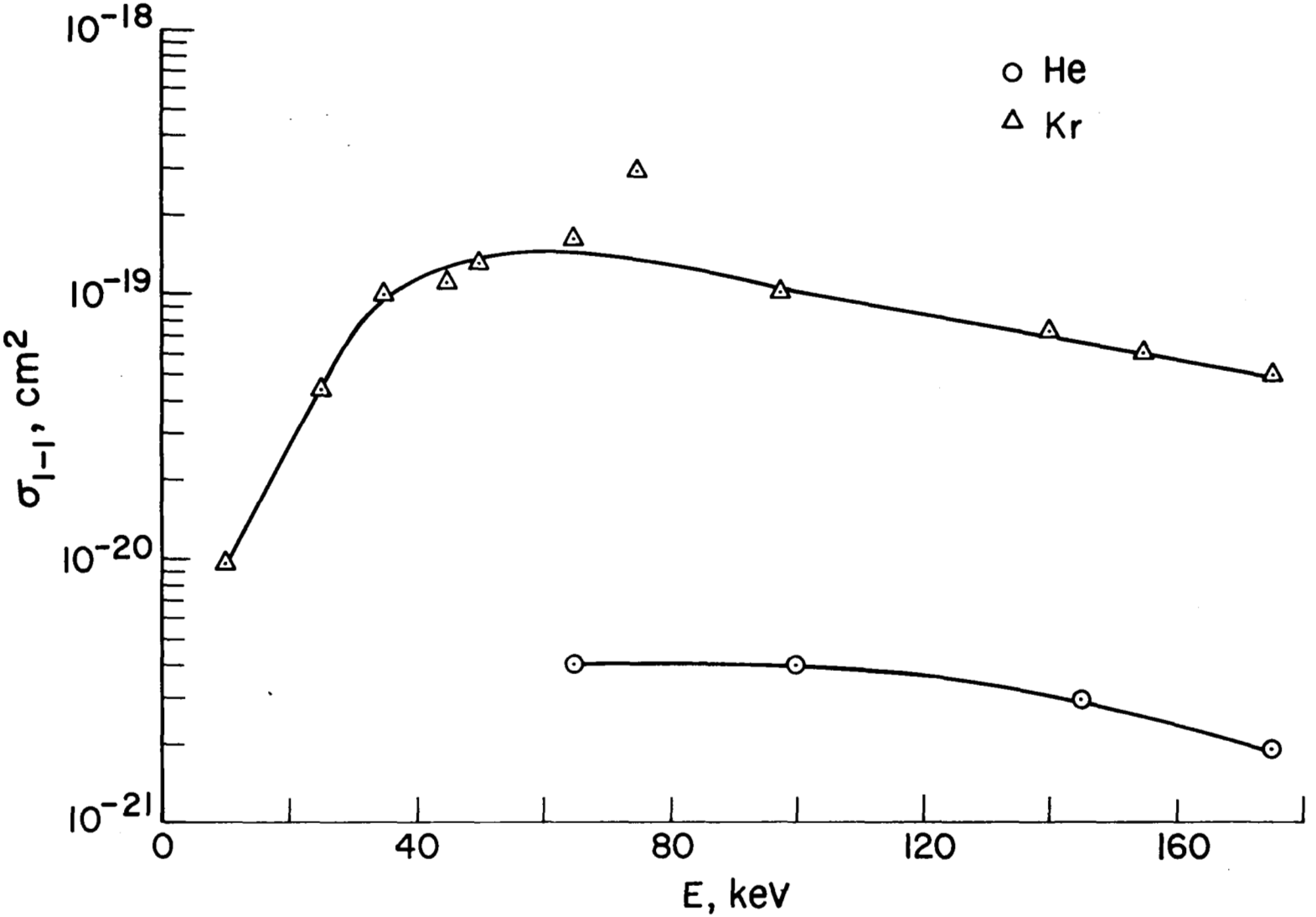

Figure 7

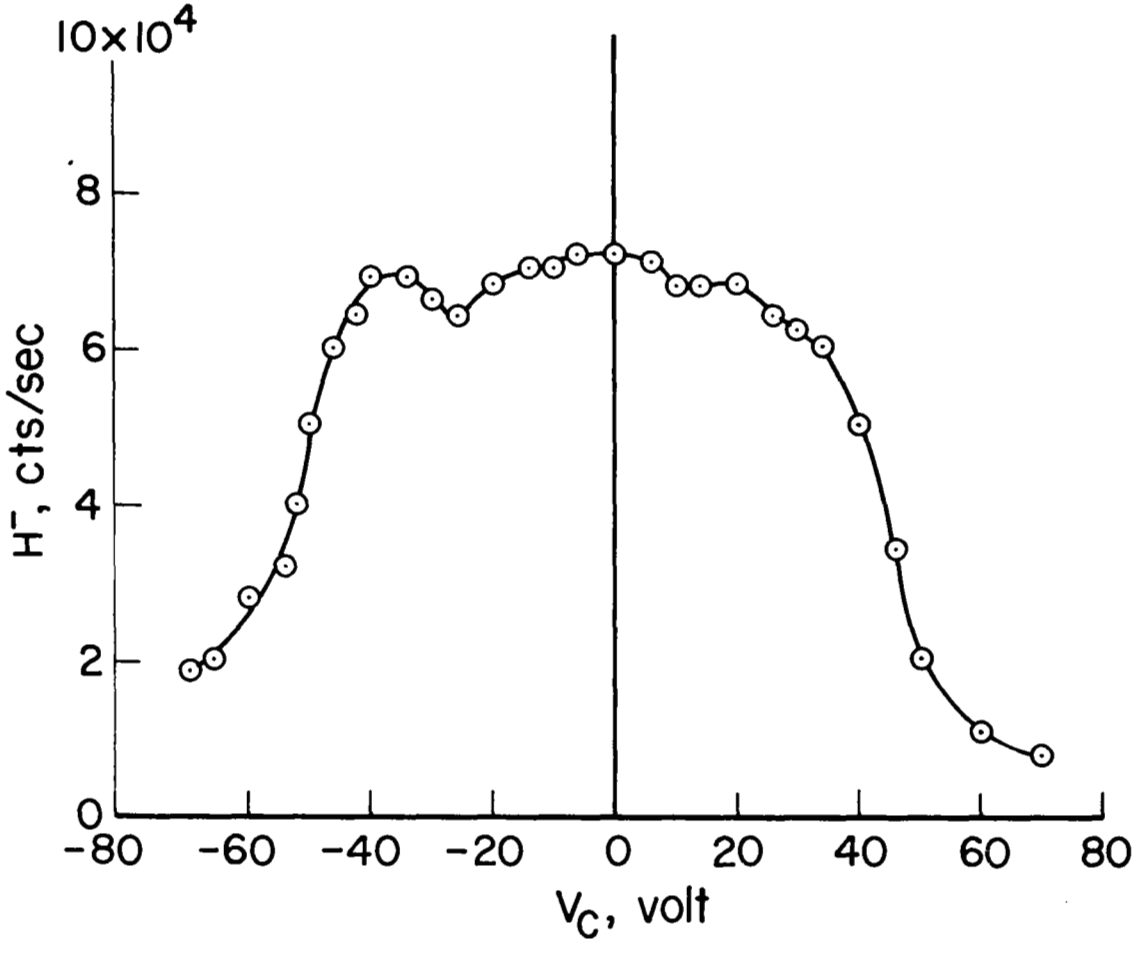

Figure 8

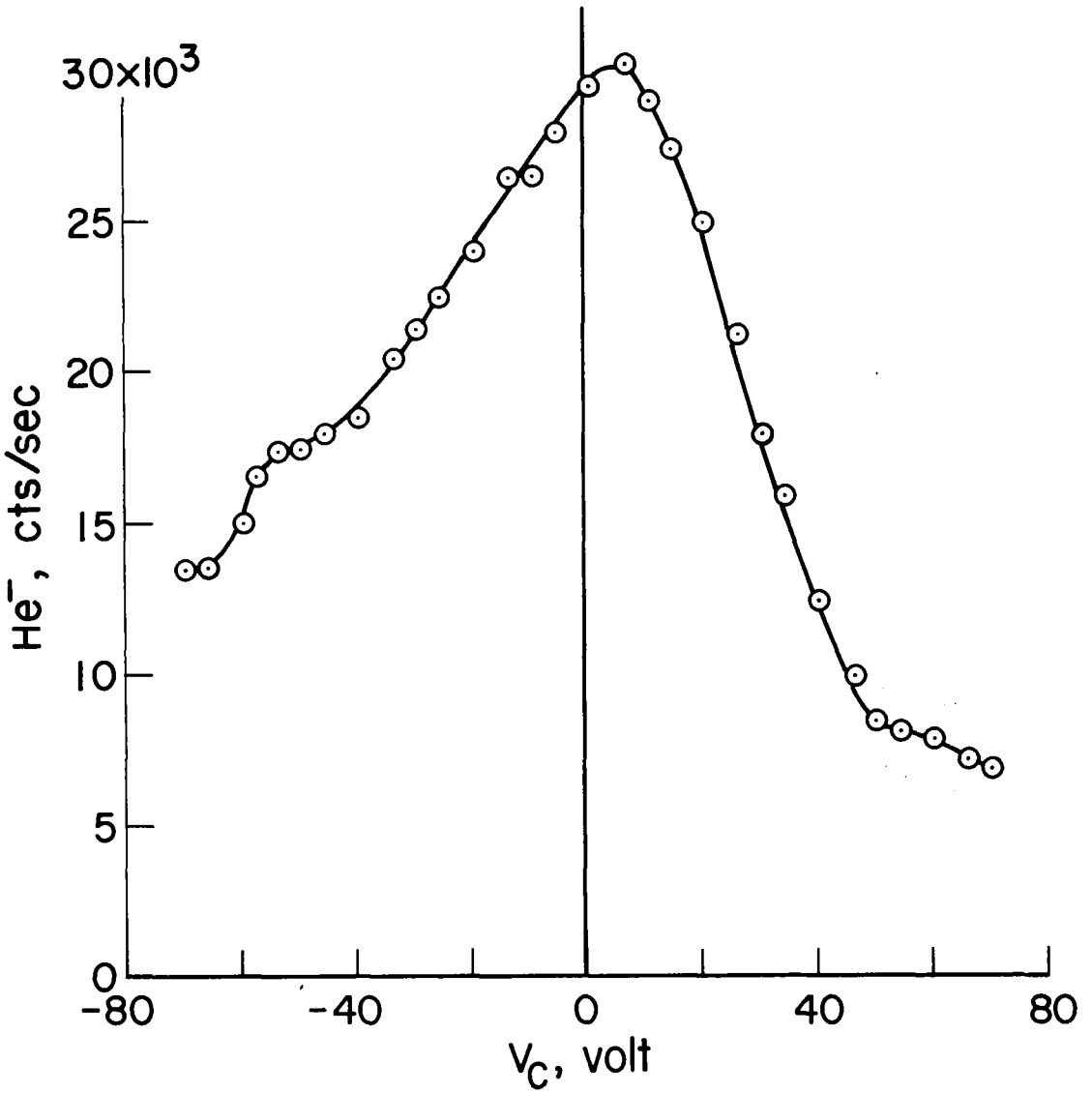

Figure 9

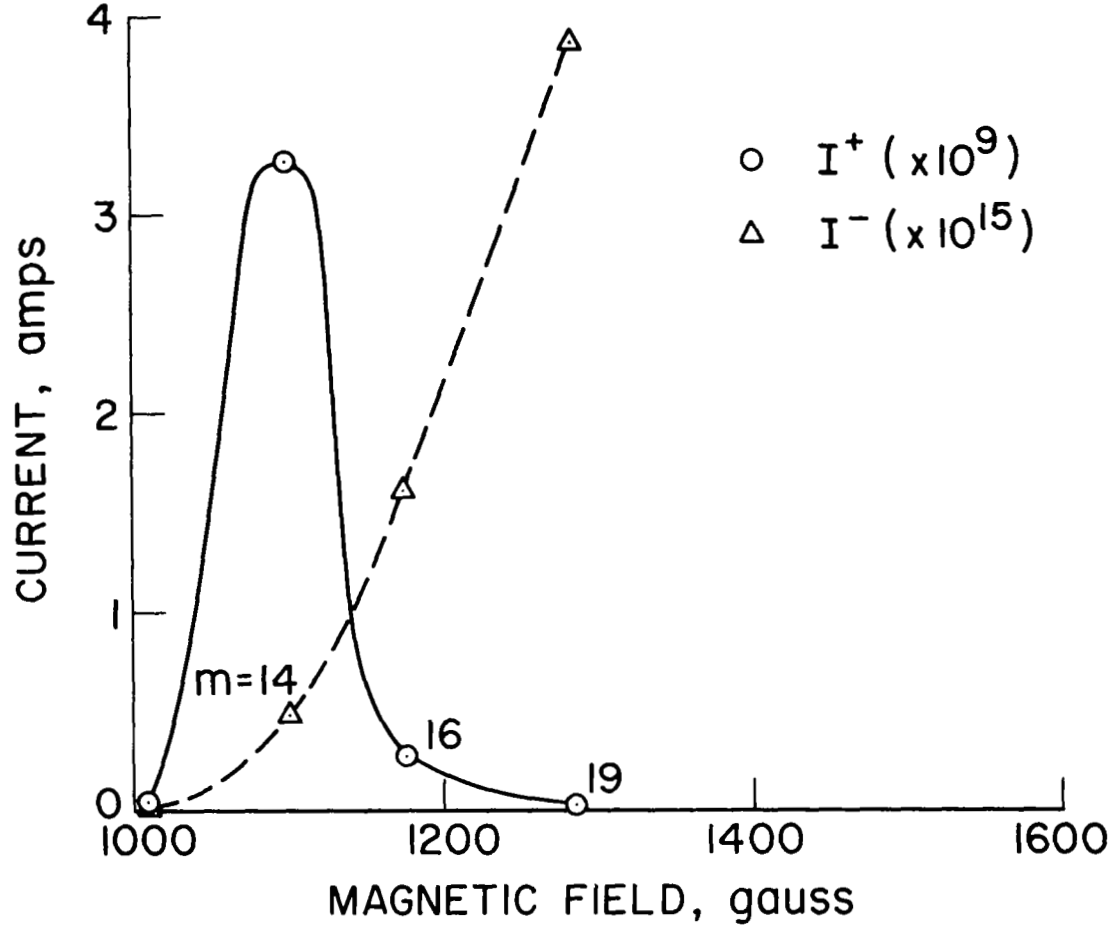
4
3
2
1
0
CURRENT, amps
1000
1200
1400
1600
MAGNETIC FIELD, gauss
m=14
16
19
I+ (x10^9)
I- (x10^15)

Figure 10

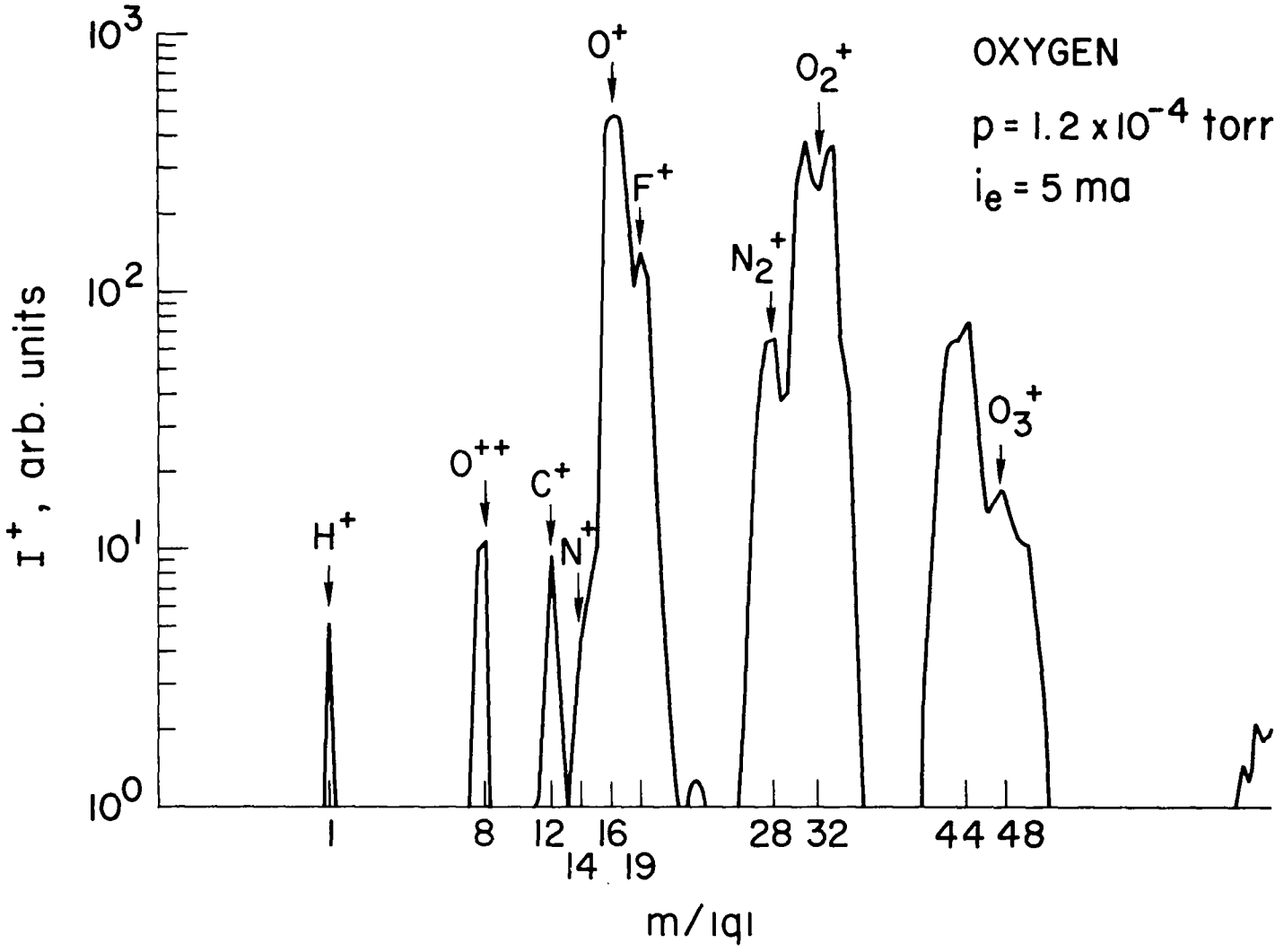
OXYGEN
p = 1.2 x 10^-4 torr
i_e = 5 ma
I+, arb. units
m/|q|
H+
O++
C+
N+
O+
F+
N2+
O2+
O3+
10^3
10^2
10^1
10^0
1
8
12
14
16
19
28
32
44
48

Figure 11

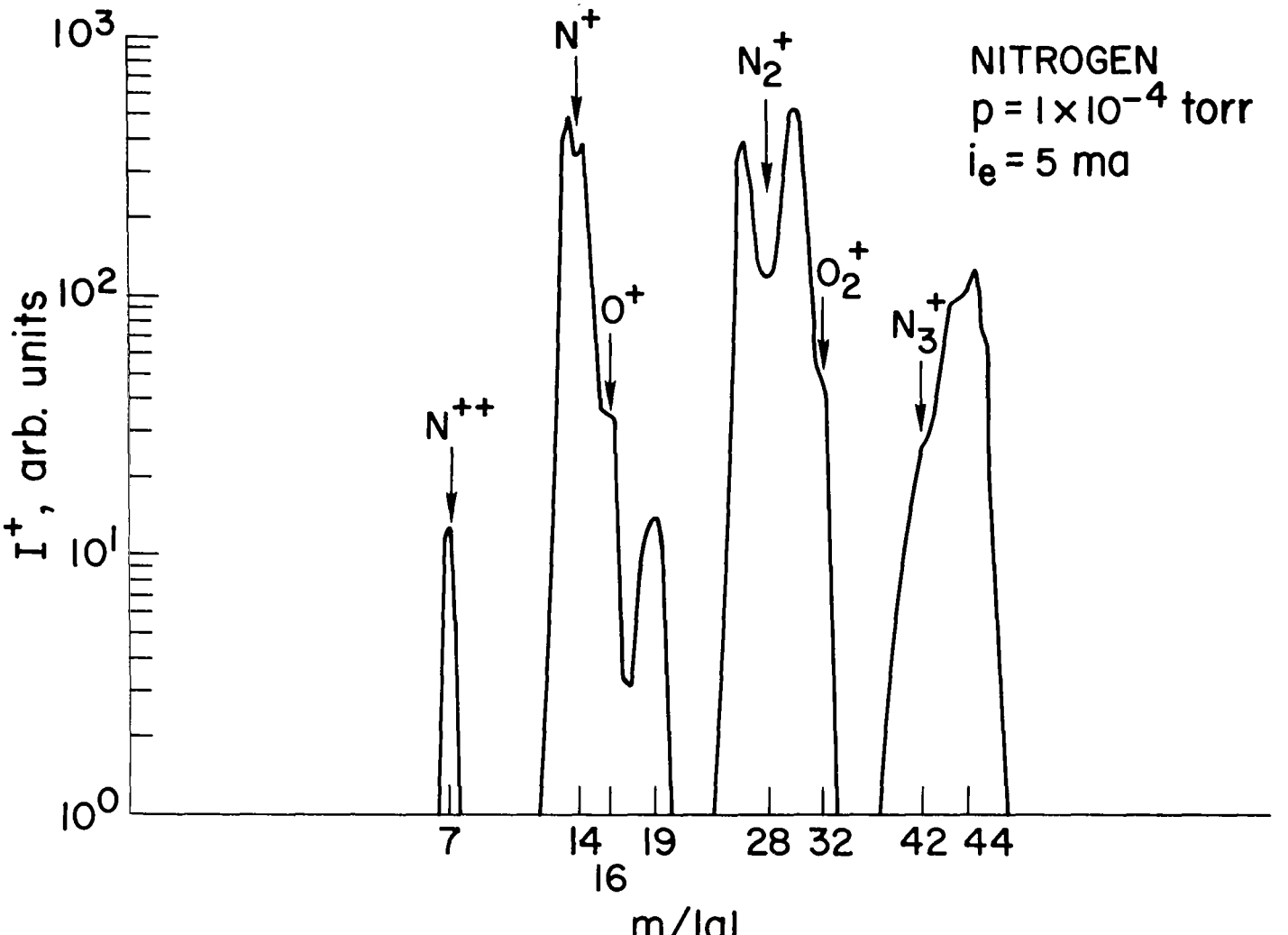
NITROGEN
p = 1 x 10^-4 torr
i_e = 5 ma
I+, arb. units
10^3
10^2
10^1
10^0
N+
N2+
O+
O2+
N3+
N++
7
14
16
19
28
32
42
44
m/|q|

Figure 12

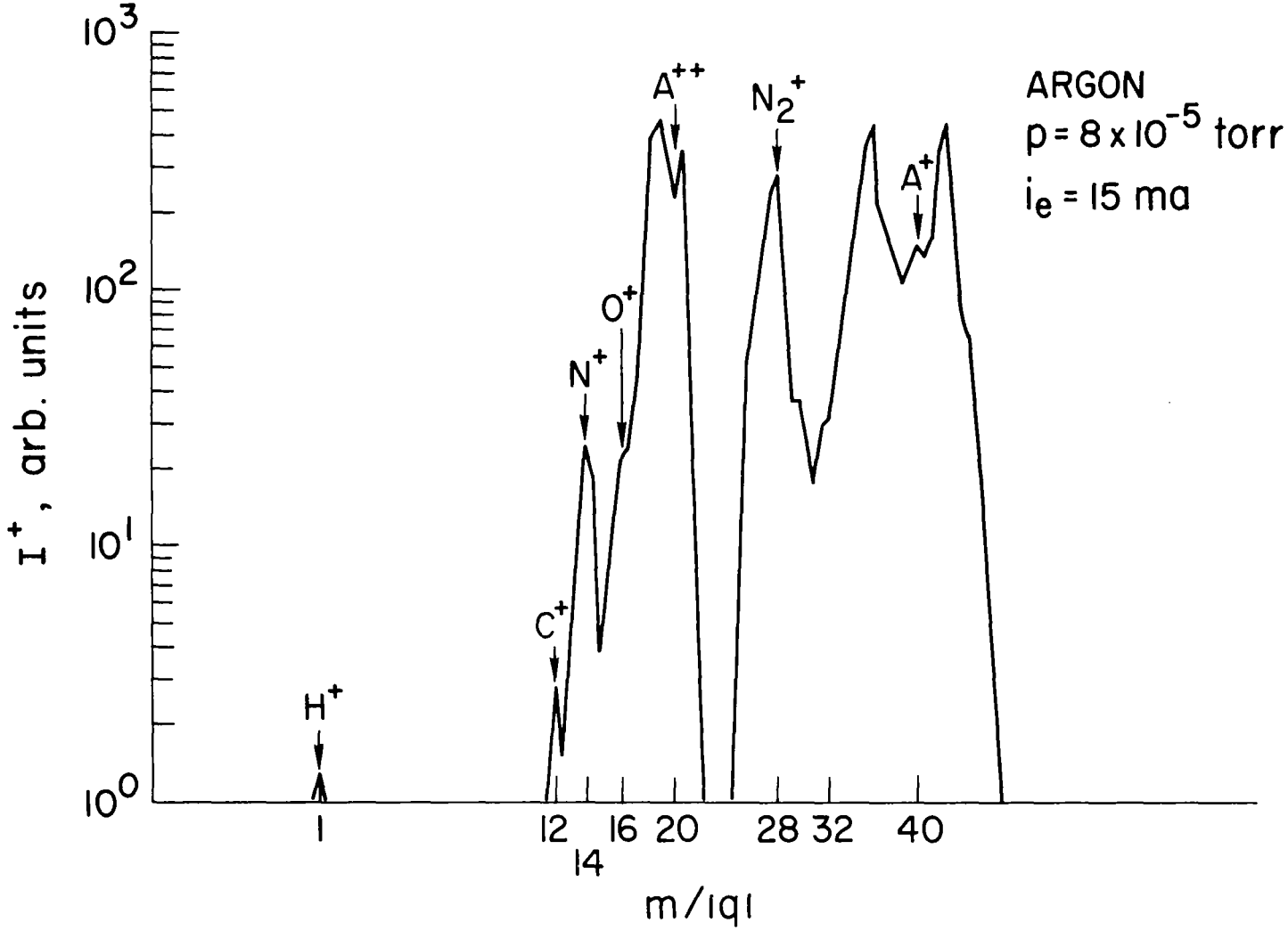
ARGON
p = 8 x 10^-5 torr
i_e = 15 ma
I+, arb. units
m/|q|
H+
C+
N+
O+
A++
N2+
A+
10^0
10^1
10^2
10^3
1
12
14
16
20
28
32
40

Figure 13

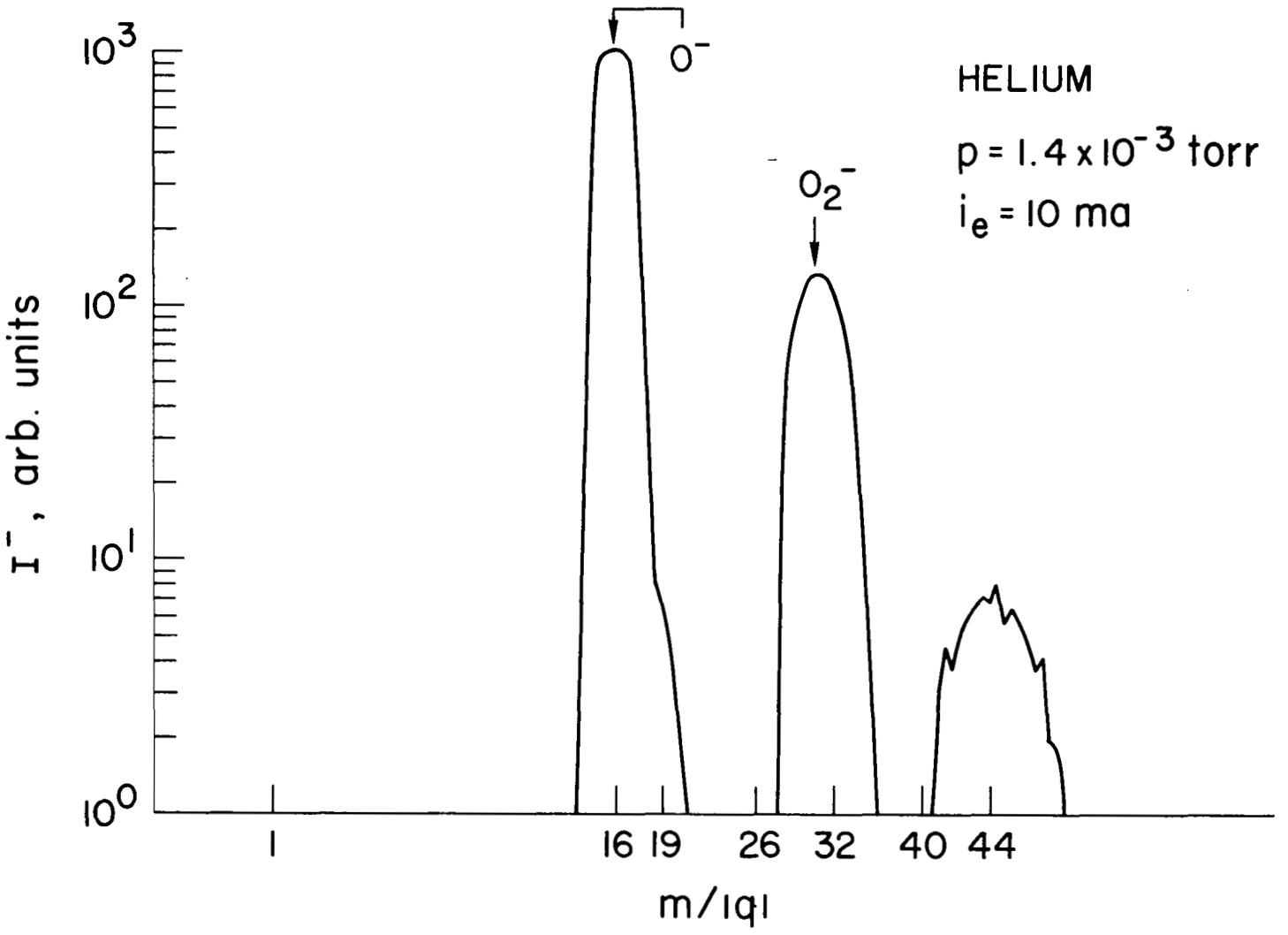
HELIUM
p = 1.4 x 10⁻³ torr
i_e = 10 ma
O⁻
O₂⁻
I⁻, arb. units
10³
10²
10¹
10⁰
1
16 19
26
32
40 44
m/|q|

Figure 14

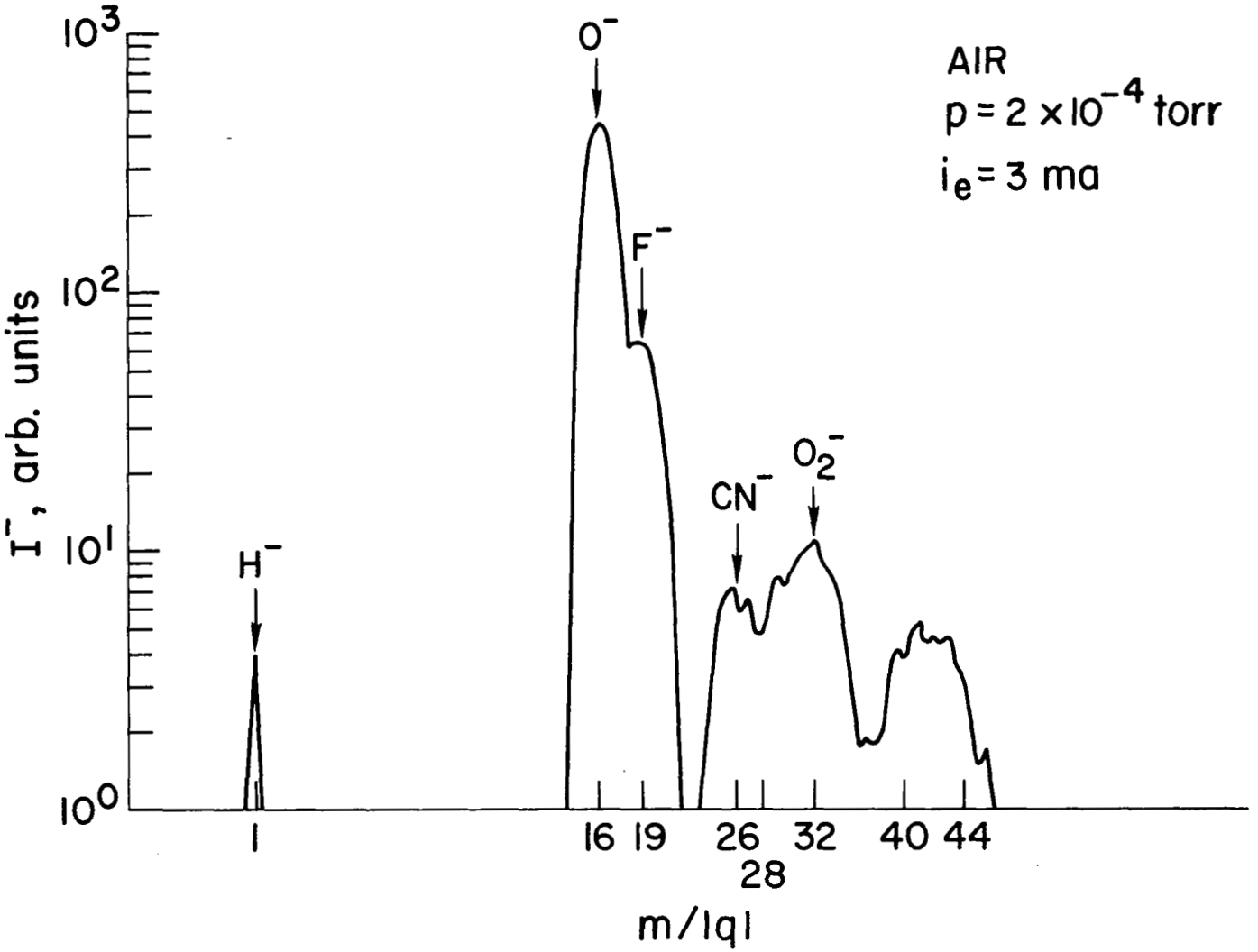
AIR
p = 2 x 10^-4 torr
i_e = 3 ma
I^-, arb. units
10^3
10^2
10^1
10^0
H^-
O^-
F^-
CN^-
O_2^-
1
16 19
26
28
32
40 44
m/|q|

Figure 15

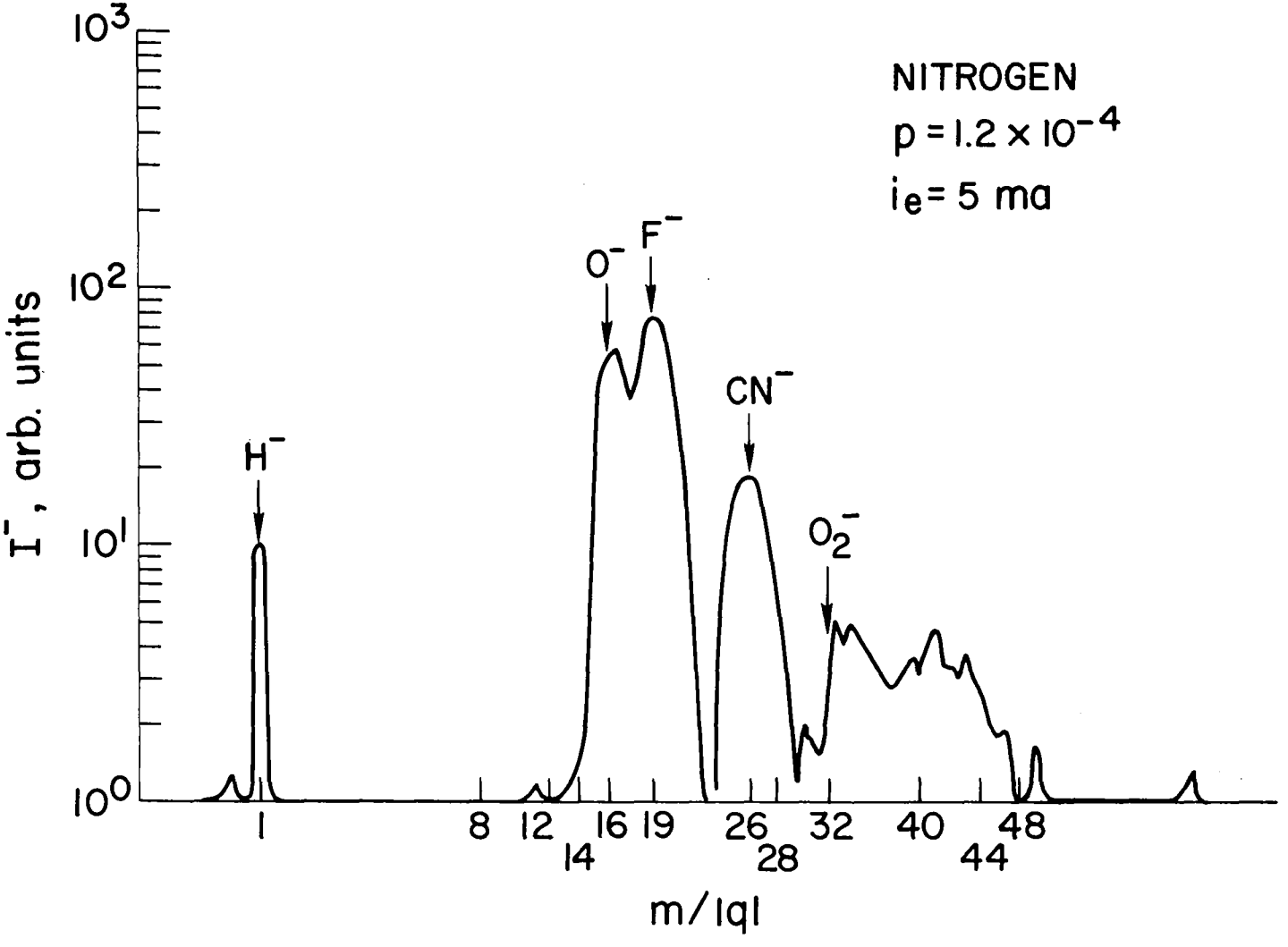
NITROGEN
p = 1.2 × 10⁻⁴
ie = 5 ma
I⁻, arb. units
10³
10²
10¹
10⁰
H⁻
O⁻
F⁻
CN⁻
O₂⁻
1
8
12
14
16
19
26
28
32
40
44
48
m/|q|

Figure 16

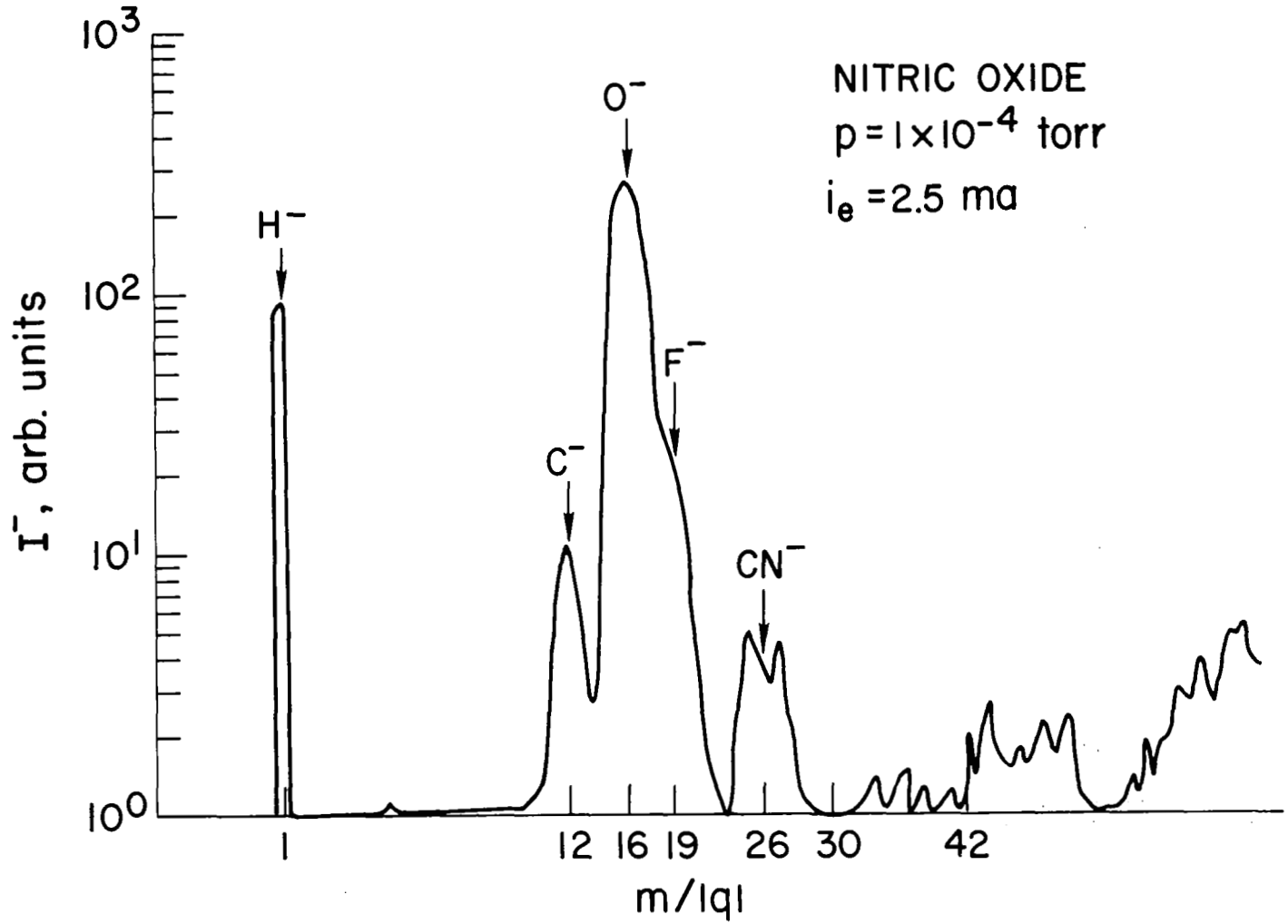
NITRIC OXIDE
p = 1 × 10⁻⁴ torr
i_e = 2.5 ma
H⁻
O⁻
F⁻
C⁻
CN⁻
I⁻, arb. units
10³
10²
10¹
10⁰
1
12 16 19 26 30 42
m/|q|

Figure 17

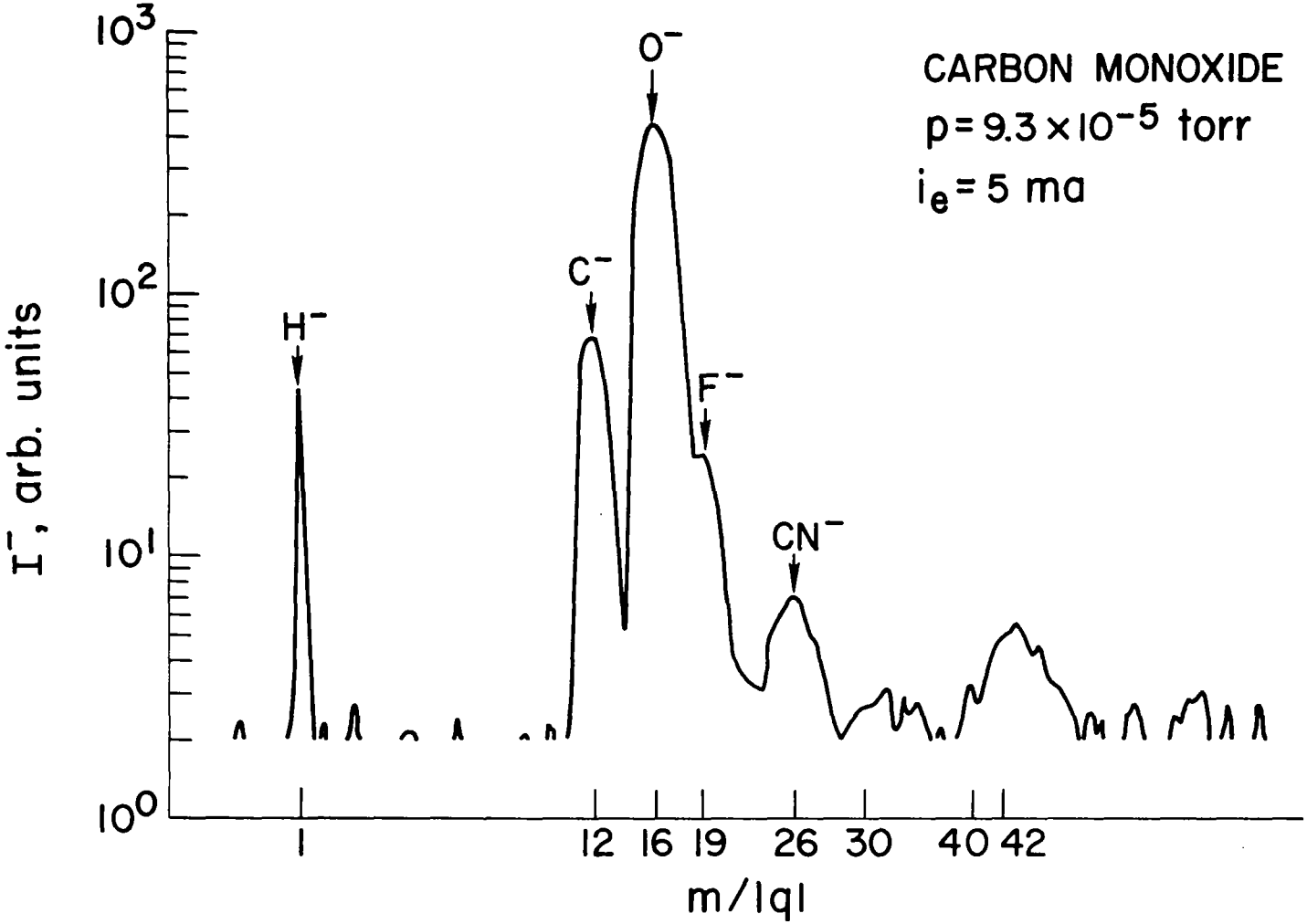
CARBON MONOXIDE
p = 9.3 × 10⁻⁵ torr
i_e = 5 ma
I⁻, arb. units
10³
10²
10¹
10⁰
H⁻
C⁻
O⁻
F⁻
CN⁻
1
12
16
19
26
30
40
42
m/|q|

Figure 18

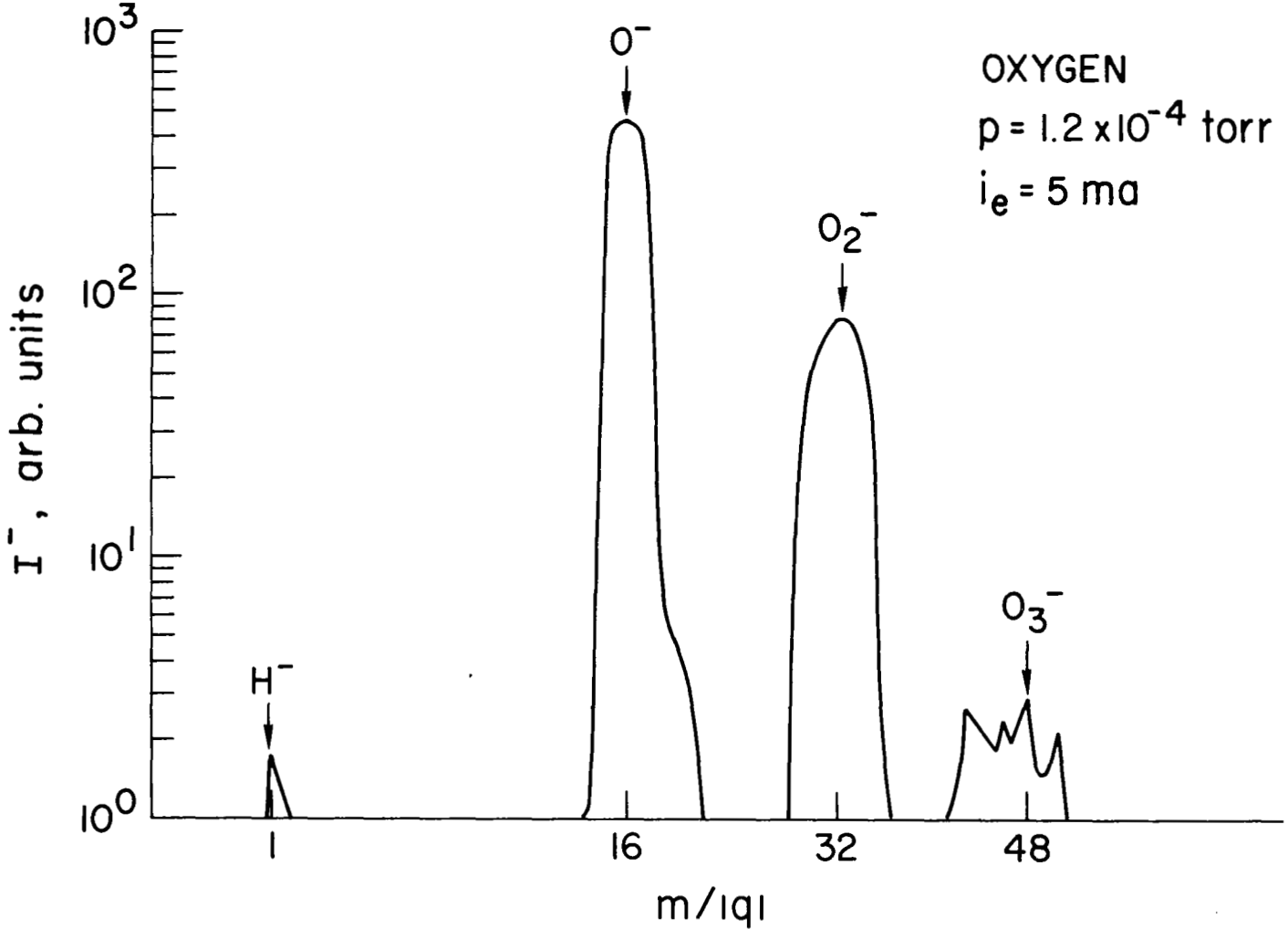
OXYGEN
p = 1.2 x10^-4 torr
i_e = 5 ma
O^-
O_2^-
O_3^-
H^-
I^-, arb. units
10^3
10^2
10^1
10^0
1
16
32
48
m/|q|

Figure 19